Flexible Multi-functional Sensors for Wearable and Robotic Applications

Mengying Xie[1], Kyohei Hisano[2], Mingzhu Zhu[1], Takuya Toyoshi[1], Min Pan[3], Shima Okada[4], Osamu Tsutsumi[2], Sadao Kawamura[4], Chris Bowen[3]*

[1]Ritsumeikan Global Innovation Research Organization, Ritsumeikan University, 525-8577, Japan
[2]Department of Applied Chemistry, Ritsumeikan University, 525-8577, Japan
[3]Department of Mechanical Engineering, University of Bath, BA2 7AY, United Kingdom
[4]Department of Robotics, Ritsumeikan University, 525-8577, Japan

Keywords: multi-functional sensors, flexible, piezoelectric, piezoresistive, optical

This review provides an overview of the current state-of-the-art of the emerging field of flexible multi-functional sensors for wearable and robotic applications. In these application sectors there is a demand for high sensitivity, accuracy, reproducibility, mechanical flexibility and low cost. The ability to empower robots and future e-skins with high resolution, high sensitivity and rapid response sensing capabilities is of interest to a broad range of applications including wearable healthcare devices, biomedical prosthesis, human-machine interacting robots such as service robots for the elderly and electronic skin to provide a range of diagnostic and monitoring capabilities. A range of sensory mechanisms are examined including piezoelectric, pyroelectric, piezoresistive and there is particular emphasis on hybrid sensors that provide multi-functional sensing capability. As an alternative to the physical sensors described above, optical sensors have potential to be used as a robotic or e-skin; this included sensory color changes using photonic crystals, liquid crystals, and mechano-chromic effects. Potential future areas of research are discussed and the challenge for these exciting materials is to enhance their integration into wearables and robotic applications.

1. Introduction

Significant progress in the development and advancement of flexible multi-functional sensors has been achieved in recent years, in particular in healthcare, robotics and biomedical areas where there is a need for high sensitivity, accuracy, flexibility and low cost. For such applications, the sensors must be compatible with large-area processing techniques and readily integrated into flexible devices, and effort in this area has accelerated the range of potential applications.[1]

Empowering robots and skins with high resolution, high sensitivity and rapid response sensing capabilities is significant to a broad range of applications including wearable healthcare devices, human-machine interacting robots such as service robots for the elderly[2,3] and electronic skin (e-skin) applied on or in the body that provide an unprecedented level of diagnostic and monitoring capabilities.[3,4] Flexible multi-functional sensors are essential components of e-skin to allow biomedical prostheses and robots to naturally interact with humans and the environment. The design and development of future e-skins has attracted significant interest in recent years, in particular an emphasis on being able to mimic the mechanically compliant yet highly sensitive properties of human skin,[4,5] multi-functional and simultaneous sensing,[6–8] and mechanical self-healing.[9] It is suggested that the modern multi-functional e-skins have great potential in non-invasive, high fidelity and continuous radial artery pulse wave monitoring.[4] They can also be used in future mobile health monitoring and remote diagnostics in cardiovascular medicine.[10]

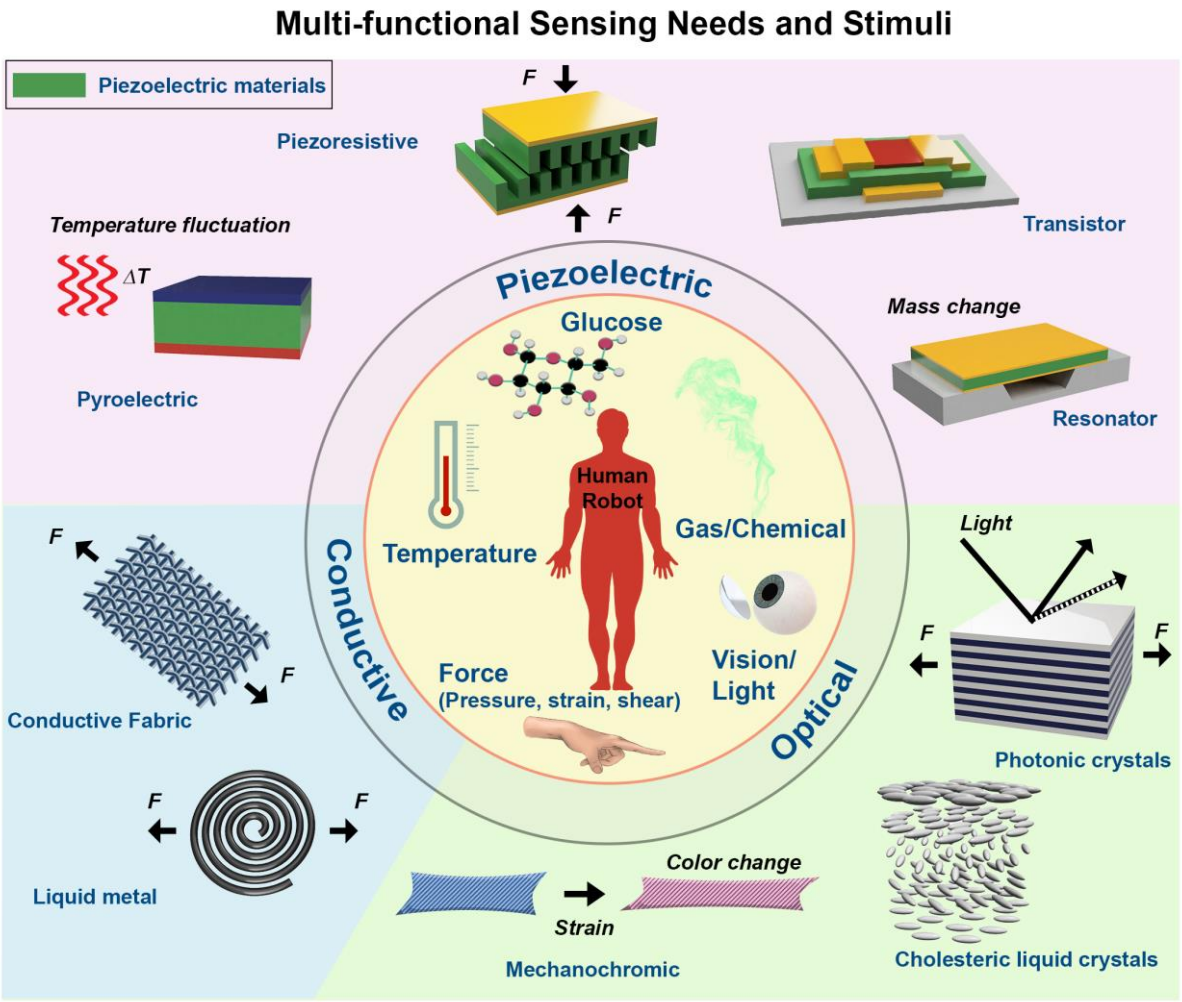

Figure 1. Multi-functional sensing needs and stimuli. Three main materials, i.e. piezoelectric, conductive and organic optical materials (photonic crystals, cholesteric liquid crystals, mechano-chromic) can achieve multi-functional sensing for wearable and robotic applications that combine sense of touch, temperature, light, and chemical detection.

Figure 1 outlines examples of the multi-functional sensing needs and stimuli. This can include pressure, strain or shear sensing using piezoelectric or piezoresistive effects or monitoring responsive color changes due to mechano-chromic effects, or using photonics or liquid crystals. Temperature can also be monitored, for example by using pyroelectric or thermochromic effects. Chemical sensing can also use piezoelectric effects, for example by monitoring mass changes using resonance.

The pressure generated by normal touch, object manipulation and human body circulation are often distributed in low-pressure regimes (<10 kPa) and medium-pressure regimes (10-100 kPa).[11] Piezoelectric pressure sensors, which develop an electric charge in response to a mechanical load, have been widely and successfully used for pressure distribution measurement. Applications including prostheses (<1 kPa),[12] diagnostics in cardiovascular medicine (< 1 kPa),[13] health care and medical diagnosis systems (< 10 kPa), [14–16] mobile blood and pulse monitoring devices (< 100 kPa),[17] wearable intelligent health monitoring bracelets (< 100 kPa),[18] portable biomedical devices and human-machine interactive robots (< 100 kPa).[19] In addition, sensors capable of operation in ultra-low-pressure regimes (< 1 Pa) also have potential in healthcare applications, for example, micro-electro-mechanical microphones and hearing aid devices.[5] Piezoelectric strain sensors have also been used measure human motion and muscle movements (drinking, swallowing and eating) to diagnose diseases or assist with rehabilitation. A range of strain sensors have been employed for a variety of applications; for example smart suits are normally equipped with sensors that operate at strains up to 55% [12,20] while sensors for detecting smiles and the blinking of an eye can operate at less than 2% strain.[12,21] To diagnose damaged vocal cords or a respiratory disorder, more accurate measurement and smaller scale strains (<0.5%) are needed to detect muscle movements during drinking and eating.[12,22]

Sensing mechanisms are not simply limited to piezoelectric effects which rely on charge generation in response to an applied stress. The pyroelectric effect leads to charge generation as a result of a temperature change and can be exploited for thermal detection, and multi-functionality is possible since pyroelectric materials are also piezoelectric. The piezoresistive effect, which corresponds to a change in resistance with strain, and triboelectric effects as a result of charge generation due to contact electrification can be also introduced to realize additional functions to form hybrid pressure or thermal sensors. In addition to pressure and

temperature sensing, piezoelectric, pyroelectric and triboelectric materials can be also used to fabricate self-powered sensors, which allows the development of next generation wireless and wearable devices[23–25] that could potentially function without any external power sources. Furthermore, piezoelectric resonators with converse piezoelectric effect have expanded their applications as novel highly sensitive biological and chemical sensors.[26,27] The sensory mechanism is based on the drift in the resonant frequency shift or the changes in the wave propagation speed due to the external stimuli. They are particularly sensitive and useful to act as electronic nose system in analogy to the human nose or for robotic molecule sensing.

Piezoresistive sensors based on conductive materials are of particular interest for applications that require a high degree of conformability and stretchability, especially in soft robotic applications.[28] Intrinsic and conductive materials coated conductive fabrics are soft, conformable and can be readily attached to, or weaved, into clothing. There is also a need for such fabrics to be waterproof and exhibit high durability. Liquid metal conductors are soft and can be fabricated into fibers[29] and planar structures[30,31]. To date, such conductive sensors can be stretched to a wide range of strains, from ~5 to 400%.

More recent developments include advanced sensing techniques such as optical sensors which rely on lens or mirror systems to transmit beams of light for sensing. These systems are of interest for medical and healthcare applications[32] and a number of biomedical optical sensors are flexible, contactless, reliable, biocompatible, non-invasive and have simple sensor-physician interfaces. Such an approach provides potential for the measurement of deformation in applications such as soft robots[33] and three-dimensional fine measurement in minimally invasive robotic surgery.[34] In particular, there is scope to exploit materials whose optical properties vary with pressure and temperature.

The review therefore aims to provide a detailed overview of the range of flexible multi-functional sensors for wearable and robotic applications. The range of sensing mechanisms covered by this review are outlined in Figure 1. Piezoelectric and pyroelectric sensors will be initially described, along with self-powered systems. Since the review aims to focus on multi-functional sensors, examples of hybrid approaches will be described, including those that combine piezoelectric and pyroelectric effects with piezoresistive, triboelectric, magnetoelectric and electro-luminscence effects, and ultimately their combination with chemical and biological sensors. Textiles with multi-functional properties will then be examined, including those manufactured from conductive materials, coated textiles and liquid metals to act as sensory elements. As an alternative to the physical sensors described above, the review will also cover the intriguing use of optical sensors within potential future e-skins. This includes color changes in response to a variety of stimuli, such as using photonic crystals, liquid crystals, and mechano-chromic effects and the challenge of integration into wearables and robotics are highlighted. **Table 1** provides a summary of multi-functional sensors in terms of active materials, mechanism, substrate, sensitivity, and their applications.

2. Piezoelectric Sensors

Piezoelectric materials are particularly attractive and have been widely used in the field of sensors [35] and actuators [36] particularly due to their high performance, and multi-functionality. Piezoelectric materials are a class of dielectric materials that can be polarized by application of external stimuli, i.e. mechanical, electrical and thermal stimulus.[37] As shown in **Figure 2**, piezoelectric materials have sub-classes of 'pyroelectrics' and 'ferroelectrics'.[38] Piezoelectrics exhibit an intrinsic electric polarization that can be reversed by an applied mechanical field. Pyroelectrics exhibit an electric polarization that can be controlled by an applied thermal field while the ferroelectrics can switch different states of electrical polarization in response to an

external electric field. All ferroelectrics are both pyroelectric and piezoelectric and all pyroelectrics are piezoelectric materials. However, not all piezoelectrics are pyroelectric, for example quartz which only becomes polarized as a result of a mechanical stress. Therefore, we can say that most of the piezoelectrics are intrinsic multi-functional materials that are capable of providing at least two functions for a particular wearable application.

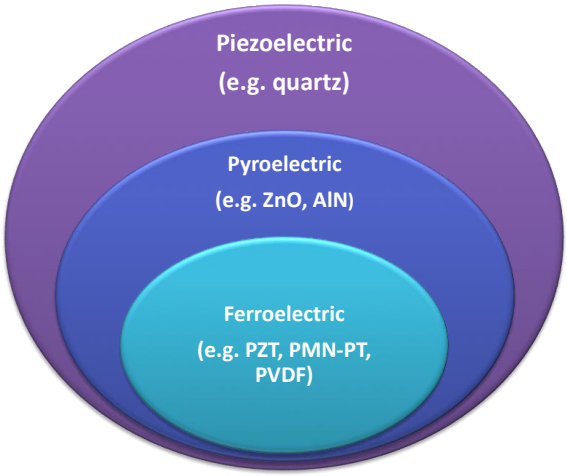

Figure 2. Relationship of piezoelectric, pyroelectric and ferroelectric materials.[38] Adapted with permission, copyright (2014), The Royal Society of Chemistry.

Multi-functional sensors that are able to simultaneously detect multiple parameters are of importance in the wearable and robotic applications. Recently, significant efforts have been paid in the development of such sensors based on piezoelectric materials. Conventional multi-functional sensors commonly involve integrating one piezoelectric sensor and other separate sensors with different sensing mechanisms on heterogeneous substrates.[39,40] However, these sensors often require a sophisticated layout of interconnections so that the volume of the devices increases. In this section, we review multi-functional sensors using piezoelectric and functionalized piezoelectric materials. A summary of the multi-functional piezoelectric sensors in terms of materials, mechanism, sensitivity and their robotic applications can be found in Table 1.

2.1. Piezoelectric and Pyroelectric Effect

2.1.1. Piezoelectric Effect

At a temperature below the Curie temperature, ferroelectric based piezoelectric materials generally often exhibit a tetragonal symmetry structure and such as asymmetric structure is associated with a dipole moment.[41] The poling process is important for ferroelectric materials as it leads to the alignment of ferroelectric domains in the direction of applied electric field and provides a net remnant polarization. It is the remnant polarization that leads to piezoelectric and pyroelectric effects. If a strain is applied along an axis of the poled piezoelectrics, the center of the cations and the center of anions are relatively displaced, resulting in a change in the piezoelectric polarization along the direction of strain in the crystal. As a result, an electric current will be induced in an external circuit and therefore the piezoelectric materials can be naturally be used for sensor and energy harvesting applications.

Equation 1 describes the direct piezoelectric effect and shows that the mechanical stress can lead to a change of electric polarization and electric field. *D* is the dielectric displacement, *d* is the piezoelectric coefficient, *S* is stress tensor, ε is the dielectric permittivity and *E* is the electric field. *i*, *j*, and *k* refers to the different direction within the piezoelectric material.

$$\mathrm{D}_i = d_{ij}T_j + \varepsilon_{ik}E_k \tag{1}$$

The piezoelectric coefficient d_{ij} is the ratio of short circuit charge per unit area flowing between connected electrodes perpendicular to the *j* direction and to the stress applied in the *i* direction. For example, when an applied strain is subjected along the 3-direction, the piezoelectric material can generate electric charge flowing through a short circuit.

$$Q = d_{33}F_3 \tag{2}$$

In addition, the open circuit voltage that is generated is

$$V = \frac{c}{ab}g_{33}F_3 \tag{3}$$

where g_{33} is the piezoelectric voltage constant that signifies the electric field developed along the 3-axis when the material is stressed along the 3-axis. The variable *a*, *b*, and *c* are the dimension of the piezoelectric materials. The relationship between d_{33} and g_{33} can be expressed as

$$d_{33} = g_{33}\varepsilon_{33}\varepsilon_0 \quad (4)$$

It can be seen that the piezoelectric sensor performance is directly related to the piezoelectric charge coefficient d_{ij}, which represents the ability to convert mechanical loads into an electric charge. Since piezoelectrics respond to dynamic forces applied to their surfaces, they are commonly used as dynamic force, touch, vibration sensors and accelerometers.[35,42,43]

2.1.1. Pyroelectric Effect

In addition, pyroelectric materials are polar dielectric materials and exhibit a spontaneous polarization, P_s, in the absence of an applied electric field or mechanical displacement.[44–46] Again, this is often achieved after poling of a ferroelectric material, as described for the piezoelectric materials above. While the piezoelectric effect originates from a change in polarization with stress, the pyroelectric effect originates from a change in the level of polarization with changes in ambient temperature. If the temperature of a pyroelectric is increased, the polarization level decreases as dipoles within the material lose their orientation due to thermal vibrations, and thus leads to a decrease in the number of charges bound to the material surface. If the pyroelectric is under open circuit condition, the free charges remain at the electrode surface and an electric potential is generated across the material. If the pyroelectric is under short circuit, an electric current flows between the two polar surfaces of the material. When the pyroelectric is cooled, the level of polarization is increased and leads to a reverse electric current flow under short circuit condition.

The relationship between the rate of temperature change *dT/dt*, generated charge *Q*, pyroelectric current *I*, surface area of the material *A*, and pyroelectric coefficient *p* under short circuit conditions with electrodes that are orientated normal to the polar direction is defined in Equation 5.

$$i_p = \frac{dQ}{dt} = pA\frac{dT}{dt} \tag{5}$$

The pyroelectric coefficient of an unclamped material under constant stress and electric field is defined by Equation 6, where P_s is the spontaneous polarization and subscripts $\sigma \; and \; E$ correspond to constraints of constant stress and electric field respectively.

$$p^{\sigma,E} = (\frac{dP_s}{dT})_{\sigma,E} \tag{6}$$

By integrating Equation 1 with respect to time, the pyroelectric charge generated due to a temperature change ΔT can be found in Equation 7.

$$Q = pA\Delta T \tag{7}$$

Since the pyroelectric material is typically an electrically insulating dielectric, the capacitance of the pyroelectric element as a parallel plate is given by Equation 8, where ε^T_{33} is the relative permittivity at constant stress, ε_0 is permittivity of free space and *h* is the thickness of the material.

$$C = \frac{A\varepsilon_3^T\varepsilon_0}{h} \tag{8}$$

Under open-circuit conditions, the pyroelectric charge produces a potential difference across the material, given by $Q = CV$, which leads to Equation 9,

$$V = \frac{p}{\varepsilon_3^T\varepsilon_0}h\Delta T \tag{9}$$

As pyroelectrics are able to respond to small changes in temperature, they have been used in the area of infrared (IR) detection and imaging of moving objects or stationary objects through a light chopper.[46] Such IR detectors are sensitive to almost the entire electromagnetic spectrum,

with a wide temperature range, a response time as short as picoseconds, and cost-effective manufacture from inexpensive materials.

2.2. Self-Powered Piezoelectric Sensors

Energy harvesters as an alternative energy source have gained significant interest since they can deliver sustainable energy to power low-power electronic devices using ambient forms of energy.[38,47–49] Self-powered electronic devices that utilize energy harvesting technology are highly desirable for next generation wireless and wearable devices, in particular in robotic applications, which require devices to be flexible and lightweight, since it enables them to operate without external power sources and eliminates the need for battery replacement and the need to manage battery supplies.[50–52] Piezoelectric materials can be directly used as self-powered sensors[49] to sense strain, force and acceleration, and the pyroelectric properties of such materials, see Figure 2, also enables them to be used as thermal sensors.[53] The most widely used piezoelectric materials for sensors and energy harvesters are hard, stiff and brittle ceramics, such as lead zirconate titanate (PZT) and lead magnesium niobate-lead titanate (PMN-PT). Although these piezoelectric ceramics have high piezoelectric performance due to their high levels of polarization, they are too brittle to be readily integrated into flexible electronics. In contrast, piezoelectric and ferroelectric polymers, in particular polyvinylidene fluoride (PVDF) and its copolymer poly(vinylidenefluoride-co-trifluoroethylene) (PVDF-TrFE) exhibit sufficient mechanical flexibility, however these polymer and composite materials possess a relatively small polarization and piezoelectric response. Therefore, advanced materials, such as flexible piezoelectric composites,[54,55] thin piezoelectric films[56] and nanofibers,[57,58] have been intensively investigated for their improved piezoelectric performance, cost-effectiveness and mechanical flexibility.

As shown in Figure 1, it is desirable for advanced sensing systems to be able to detect multiple stimuli. A typical piezoelectric sensor has three types of sensing modes, i.e. longitudinal (d_{33}), transverse (d_{31}) and shear (d_{15}), depending on the way a piezoelectric material is cut or polarized. It is relatively easy to produce either longitudinal or transverse sensors based flexible piezoelectric[59,60] since the same electrode can be used for poling and sensing operations. However, the design and manufacture of shear force sensors continues to be a challenge as it requires a more complex configuration or device structure since the electrodes are applied normal to the direction of polarization. In order to sense a range of forces, a freeze casting technique as a cost-effective approach has been used to fabricate arbitrary sensor configurations. Xie, *et al.* developed self-powered flexible and highly active lead zirconate titanate-polydimethylsiloxane (PZT-PDMS) composite sensors able to detect pressure and shear forces.[54] **Figure 3a** shows that the lamellar PZT structure was initially developed via freeze-casting and piezoelectric composite was formed by impregnating a PDMS matrix into the aligned pore channels. This flexible PZT-PDMS composites provides the advantages of flexibility from polymer matrix and piezoelectricity from the connected PZT fillers, exhibits an exceptional high effective d_{33}^* of 750 pC/N and is able to bend to a small radius of 8 mm and maintain a high d_{33}. With different configurations, the self-powered sensors are able to detect longitudinal, transverse and shear loads. In addition, with a single piezoelectric sensor it is possible to detect various mechanical stimuli over a broad sensing range.

Maity, *et al.* presented an all-organic sensor based on electrospun PVDF nanofiber mats. Continuous electrospinning has been used to fabricate a multilayer PVDF nanofiber mat and poly(3,4-ethylenedioxythiophene) (PEDOT) was coated as electrodes via a facile vapor-phase polymerization.[57] This multilayered structure was able to achieve a high energy conversion efficiency of 66% and the self-powered sensor was able to sense human movement (such as foot strikes and walking) and machine vibration. In addition to self-powered mechanical

piezoelectric sensors, thermal pyroelectric multi-functional sensors have also been studied. Temperature fluctuations can be found everywhere in daily life, such as the temperature difference between the human body and the ambient environment. In particular, in the winter the temperature difference, can reach up to 60 ºC. During the breathing process, temperature differences between the human body and ambient atmosphere and the water vapor in the exhaling gas can create a region with a remarkable time dependent temperature fluctuation at the area around the mouth. Xue, *et al.*[61] developed a wearable pyroelectric nanogenerator in a respirator for energy harvesting of human respiration with a flexible PVDF thin film, as shown in Figure 3b. This pyroelectric nanogenerator was able to generate a maximum power of 8.31 μW at a load resistance of 50 MΩ when the ambient temperature was 5 ºC. This nanogenerator acted as a self-powered sensor to monitor the respiratory rate and intensity, thus could potentially monitor the outdoor health status of the elderly and those at risk of potential diseases. In addition, under a constant respiratory sate, the pyroelectric generator also acted as a sensor for ambient temperature monitoring.

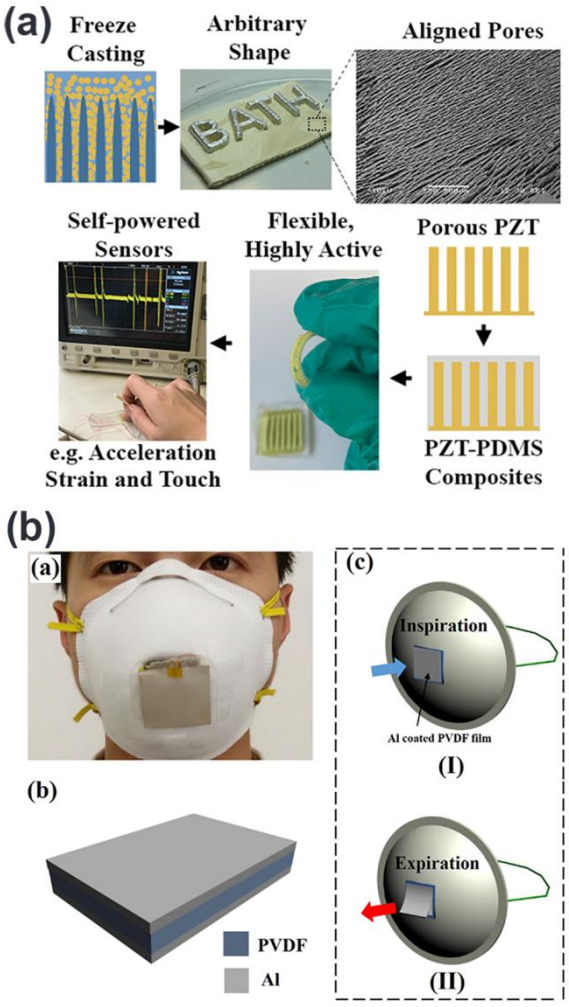

Figure 3. Self-powered piezoelectric and pyroelectric multi-functional sensors. a) Flexible self-powered piezoelectric sensors to detect pressure and shear forces.[54]. Reproduced with permission, Copyright (2018), The Royal Society of Chemistry. b) Pyroelectric breathing sensor attached to a respirator and the sensor driven by human respiration. Reprinted from ref. [61], Copyright (2017) with permission from Elsevier.

2.3. Hybrid Piezoelectric Sensors

The multi-functional sensors described in section 2.2 operate on the basis of a single mechanism, either based on the piezoelectric or pyroelectric effect. These sensors are able to sense multiple signals based on one type of physical quantity; however they are often limited in performance for the detection of multiple parameters and are unable to meet the requirement of multi-purpose or multi-functional sensors. Studies have shown that the epidermis of human skin has a permanent electric dipole moment perpendicular to its surface and can be treated as a piezoelectric and pyroelectric sensor layer.[62,63] For future intelligent sensing systems, the

development of artificial flexible e-skins that are able to mimic the comprehensive perceptive functions of human or animal skin, namely sensing of force, temperature, smell and vision ability remains a topic of intense interest and presents significant challenges for the applications in robotics, artificial intelligence and human-machine interfaces.[3,10]

2.3.1. Piezoelectric & Pyroelectric Systems

All pyroelectrics are piezoelectric materials, see figure 2, thus they are naturally treated as ideal choice for simultaneously sensing both mechanical and thermal stimuli. Common piezoelectric and pyroelectric materials including zinc oxide (ZnO),[64–66] PVDF,[65,67,68] and PMN-PT [69] have been investigated for mechanothermal sensors. ZnO and PVDF have relatively low piezo- and pyro-coefficients (ZnO: d_{33}~ 12.4 pC/N, p~-9.4 $\mu Cm^{-2}K^{-1}$; PVDF: d_{33}~ -33 pC/N, p~-27 $\mu Cm^{-2}K^{-1}$).[38,44] Studies showed that incorporation of ZnO in PVDF matrix can significantly improve the piezoelectric and pyroelectric properties of PVDF.[70] ZnO has been reported to play an important role in enhancement of the dielectric constant of the ZnO/PVDF composites and increases the conductivity of the polymer and leads to a more efficient poling process by reducing the required electric field. Therefore, Lee, *et al.*[65] developed a free-standing ZnO nanorod-PVDF composite thin film on a reduced graphene oxide (rGO) treated polyethylene terephthalatae (PET) thin electrode and claimed that this sensor was the first to simultaneously monitor both pressure and temperature. This ZnO/PVDF pressure sensor was able to react to a minimum pressure of 10 Pa which is 10^3-fold lower than the minimum level required for artificial skin. In [68], barium titanate ($BaTiO_3$) nanoparticles were embedded in PVDF-TrFE to improve sensitivity to touch and temperature. This composite shows a linear trend with a high sensitivity to temperature up to 54 pF/ºC and pressure sensitivity of 0.22 nF/N , see Table 1.

For piezoelectric and pyroelectric sensors, another approach to increase sensitivity is to use materials with higher piezoelectric and pyroelectric coefficient. Single-crystal PMN-PT as a

highly active piezoelectric material possess a ultrahigh d_{33} of 2800 pC/N,[71] which is 85 and 226 times higher than that of PVDF and ZnO, respectively; the material also exhibits a high pyroelectric coefficient of 1040 $\mu Cm^{-2}K^{-1}$.[44] A number of attempts have been made to fabricate highly active flexible PMN-PT[69,72] and Chen, *et al.* used flexible single crystal 0.7PMN-0.3PT ribbons to both realize motion and temperature monitoring [69]. **Figure 4** demonstrates the fabrication process of this 0.7PMN-0.3PT ribbon-based hybrid sensor on flexible polymer substrate. This flexible PMN-PT sensor attached to the human skin enables high sensitivity for human body motion and can precisely detect acoustic signals.[69] In addition, the sensor was used for monitoring temperature related activities, such as warm water flow and light illumination.

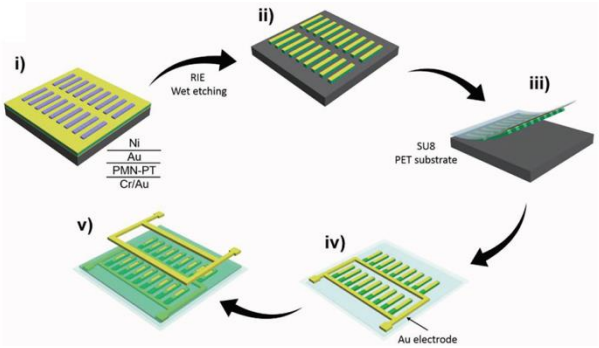

Figure. 4. Multi-functional sensors combined piezoelectric and pyroelectric effect. PMN-PT ribbon-based sensor for water temperature and light illumination monitoring. Reprinted from ref. [69] with permission from John Wiley & Sons.

2.3.2. Piezoelectric & Piezoresistive Systems

The above are examples of multi-functional sensors with piezoelectric and pyroelectric mechanisms. In some cases, while piezoelectric materials have been used, additional mechanisms such as piezoresistive and triboelectric effects can also be introduced to realize additional functions. Suen, *et al.* developed an e-skin with interlocked ZnO nanorods[66] that was able to measure and monitor arterial pulse pressure and temperature, see **Figure 5a**. By using a controlled temperature and reaction time, high-aspect-ratio ZnO nanorods were grown vertically on the surface of a PDMS substrate as top and bottom electrodes. The sensing

mechanism of this ZnO sensor is not based on piezo- or pyro-electric effects but depends on the pressure-induced change in contact resistance between interlocked high-aspect-ratio nanorods and thermo-resistance under different temperature. Under a static and dynamic pressure, the tactile sensor exhibited a high pressure sensitivity of -0.768 kPa^{-1}, see Table 1. In addition, the e-skin had a high thermal sensitivity of -0.70 %/ºC and lower activation energy for electrical conduction of charge carriers (0.155 eV). Some multi-functional sensors couple piezo- and pyro-electric effects with the piezoresistive effect. In figure 5b, a composite piezoelectric layer based on lithium-doped ZnO nanowires embedded in PDMS has been used as a dynamic piezoelectric sensing element. The element was sandwiched between two functionalized electrodes based on PEDOT:PSS coated silver nanowire (AgNWs) electrodes embedded in PDMS.[64] The electrodes acted as static motion and temperature sensing element for the multi-functional sensor.[64] Physical monitoring of blood parameters, namely blood temperature and input pressure and frequency of the pulsed fluids, is of interest in medical practice and sport, therefore a self-supporting vessel-like structure was developed to simulate electronic blood vessels,[67] as shown in figure 5b. The structure consisted of a single-walled carbon nanotube (SWCNT) electrode, a modified ZnO piezoresistive temperature sensing array, PVDF piezoelectric nanofibers as pressure and bending sensing elements and a silver electrode on braided cotton hose substrate. This electronic vessel showed a high temperature sensitivity of -0.025 $\Delta R/R/ºC$ over a wide temperature range (25ºC - 65ºC), see Table 1.

Human skin is a complex sensory system that contains unique epidermal and dermal microstructures and sensory receptors. In order to mimic the interlocked ridge structures between dermal-epidermal layers of human fingertip, Park, *et al.*[73] proposed a single-layer interlocking e-skins with PVDF and reduced graphene oxide (rGO) microdome structure, see the left two images in Figure 5c. As a result of the piezoelectric and piezoresistive nature of the PVDF-rGO composites, this human skin-inspired e-skin was able to perceive and differentiate

static and dynamic pressure, such as temperature dependent pressure monitoring of artery vessels, acoustic sound detection, and surface texture recognition of various surfaces. Fingertip-like microridge patterns on the surface and interlocked microdome arrays were used to amplify tactile signal by pressure, temperature and vibration.[73] This artificial fingertip was able to detect normal forces with sensitivity of 35 μA/Pa (<2.45 kPa) and 5 μA/Pa (2.45 to 17.15 kPa), detect skin temperature with sensitivity of 3.3 %/°C, which can be found in Table 1.[73] Based on Park's work, Lee, *et al.*[55] fabricated an e-skin with three stacked interlocked microdome layers, which is demonstrated in Figure 5d. This multilayer structure that consisted of interlocked microdome arrays enabled an ultrahigh sensitivity of 47.7 kPa^{-1} over an exceptional broad pressure monitoring range from weak gas flow, acoustic sound, to foot pressure (0.0013-353 kPa), see Table 1. In addition, this sensor exhibited a linear response over a broad sensing range which simplified the sensing system without additional signal processing, enabling device miniaturization and low power consumption. Later, the same research group developed a readout integrated circuit and mobile monitoring interface for this triple-mode microdome e-skins[74] in order to detect and monitor three different signals separately and realize wireless communication.

Furthermore, piezoelectric, piezoresistive and triboelectric effects can be combined to realize a dual-function mechanical sensor to detect human swallowing, waking gaits, finger flexure and finger tapping.[58] As shown in Figure 5e, a carbonized electrospun polyacrylonitrile/$BaTiO_3$ (PAN-C/BTO) nanofiber mat was encapsulated in PDMS to form a dual-function sensor. This sensor was able to (i) detect curvature based on the impedance change of the conducting nanofiber and (ii) detect pressure via the $BaTiO_3$ nanoparticle enhanced singe-electrode triboelectric nanogenerator independently. The pressure sensing mechanism is shown in Figure 5e, where carbonized PAN nanofibers are electrodes, and $BaTiO_3$ nanoparticles in nanofibers of PDMS acts as a negative triboelectric friction layer.

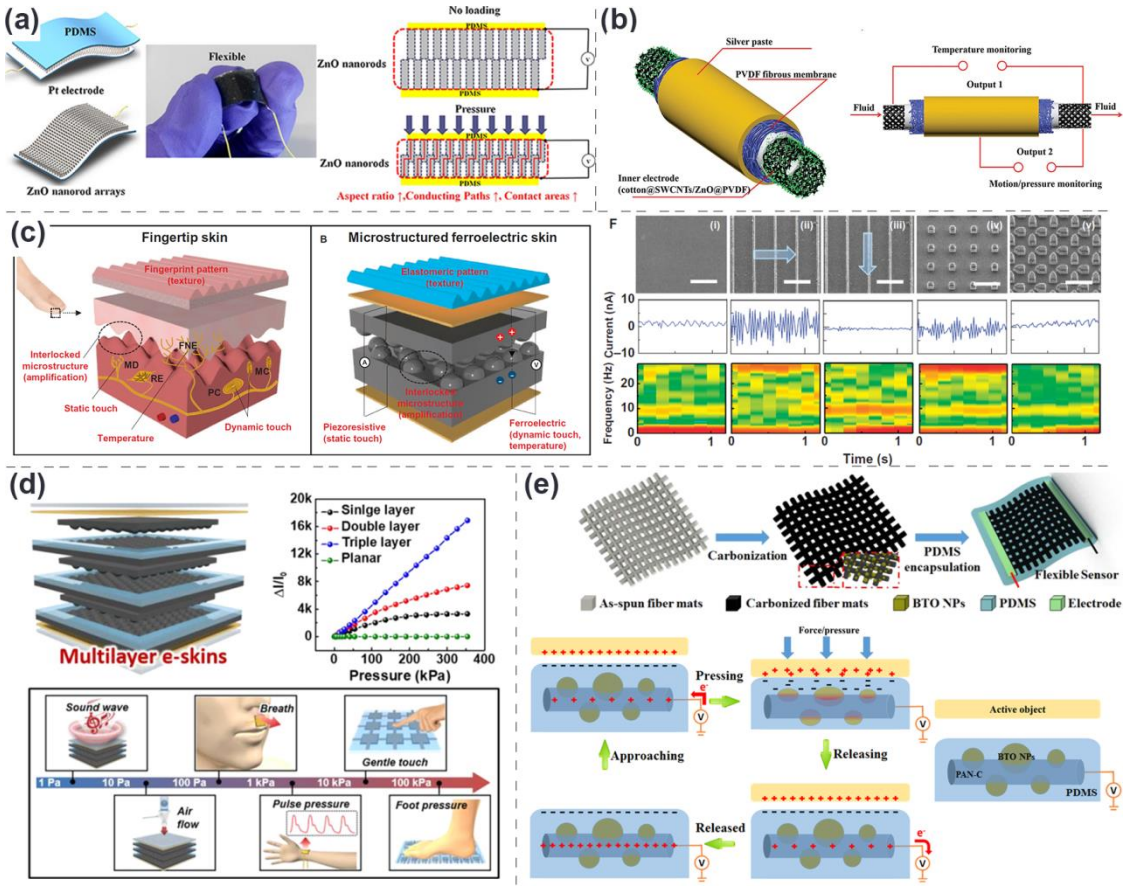

Figure 5. Multi-functional sensors combined piezoelectric and piezoresistive effect. a) Schematic and mechanism of flexible tactile sensor using interlocked ZnO nanorods. Reprinted from ref. [66], Copyright (2018), with permission from Elsevier. b) Schematic illustrates the cotton@SWCNTs/ZnO@PVDF structure-based electronic vessel that capable of monitoring of temperature, motions and liquid flow. Reproduced from ref. [64] with permission from The Royal Society of Chemistry. c) Triple-mode flexible PVDF/RGO composite bio-inspired e-skin sensor. Reprinted with permission from ref. [73]. Copyright 2015, AAAS. d) Multilayer piezoelectric e-skin that can monitor diverse stimuli from a low to a high pressure range and exhibit linear response over an exceptionally broad pressure range. Reprinted with permission from ref. [55]. Copyright (2018) American Chemical Society. e) The fabrication process and working mechanism of the flexible dual-function PAN-C/BTO self-powered pressure sensor. Adapted with permission from ref. [58]. Copyright (2018) American Chemical Society.

2.3.3. Piezoelectric & Other Systems

In addition to pyroelectric and piezoresistive effect, the piezoelectric effect has been integrated with other mechanisms, including electrostatic, magnetic and photo-electric. Regarding the electrostatic mechanism, Kimoto, *et al.* proposed a novel tactile sensor based on a pair of PVDF films, which enables identification of hardness, thickness and shape of materials.[75] When the front electrode of the PVDF film was grounded, the contact voltage on the back electrode

induced by the piezoelectric effect depended on the hardness and viscosity of the object. When the back electrode was grounded, the contact voltage induced by the electrostatic effect depended on the electrostatic property of the object and the piezoelectric effect. If both PVDF back electrodes are grounded, the electrical properties, such as capacitance of the testing material, can be measured.[75]

Magneto-electric coupling composites possess both a magnetostrictive phase and piezoelectric phase, and their electric polarization can be controlled by the external magnetic field or electric field.[76,77] For example, Sang, *et al.* fabricated a piezoelectric polyvinylindene fluoride/carbonyl iron (PVDF/CI) magnetic composite film[77] by dispersing carbonyl iron magnetic particles into PVDF matrix through a solution casting process, see **Figure 6a**. On increasing the applied magnetic field, the amount of piezoelectric charge also simultaneously increases and the magnetic flux density and magneto-electric charge signals follow a polynomial curve, therefore this composite film can be used as a dual function sensor for mechanical deformation and magnetic field.

ZnO is a semiconductor with a wide band-gap, high exciton biding energy, ultraviolet (UV) light sensitivity and good piezoelectric performance. Interconnected networks of ZnO nano- and micro-tetrapods have been deposited between two gold electrodes as a UV photodetecting and hydrogen sensing element.[78] The material exhibited a significantly high photocatalytic activity against methylene blue under UV light, and was able to completely degrade the dye in 10 min. The coupling effect of piezoelectric polarization, semiconductor properties and photon excitation under external strain on the piezo-phototronic semiconductors leads to a piezo-phototronic effect.[79] For instance, under the application of an external strain, the positive local piezo-charges around the interface of piezo-phototronic semiconductors, such as ZnO/NiO, can lower the energy band near the interface between ZnO and NiO and thus lead to a significant

increase in output current. The photon-excited excessive carriers are rapidly separated by the built-in electric field then contribute to enhance the junction current.[79] Human/machine interfaces are not limited to only mechanical considerations, since vision is also critical. Vision based artificial e-skins are of importance as they enable have the potential to mimic complex functionalities of retina and enhance, or even replace, vision ability. A self-powered vision e-skin based on a pixel-patterned matrix of piezo-photo-detecting PVDF/Ppy film can be attached to human skin and actively output a piezoelectric voltage under applied deformation, and the output signal is significantly influenced by UV illumination. The piezoelectric output can act as both photodetecting signal and electrical power. This wearable photodetector system can be used in the fields of smart glasses and multi-functional contact lenses, which enhance or replace human vision.[80]

In addition, electroluminescence (EL) has been coupled with piezoelectric effect. EL devices have been used as a liquid crystal display backlight, and as architectural and decorative lighting based on phosphor excitation, where hot electrons are injected from a dielectric layer to a phosphor layer when a high electric field is applied to a phosphor layer.[81] Piezoelectric ceramics as dielectric materials can be used as an insulating layer in EL devices and the piezoelectric effect is also capable of providing electric current to the EL device.[82,83] Lee, *et al*. developed a tri-function piezoelectric phosphor device for the first time based on the all-powder processing methods using ZnS powder as a phosphor layer and piezoelectric PZT[82] and PVDF[83] (see figure 6b) as the dielectric layer, respectively. In one mode of operation, under the application of a sinusoidal external voltage, the device could generate light and sound based on the EL and piezoelectric effect respectively. In another mode of operation, by dropping a weight onto the surface of EL device, it was able to produce the piezoelectric-driven EL light by converting the mechanical pressure into optical energy. In Lee's work,[83] the device

achieved the best-record luminous efficiency of 10 lmW^{-1} at 100 V and 400 Hz, and the sound pressure levels are linearly increased.

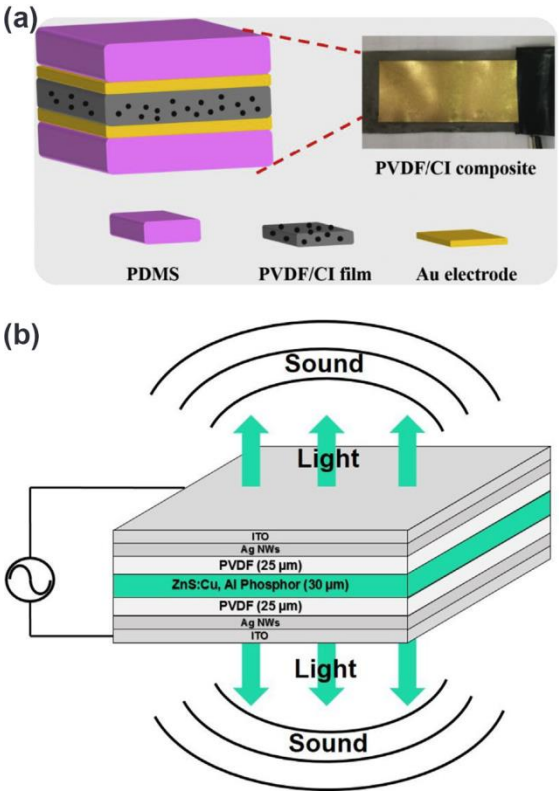

Figure 6. Multi-functional sensors with piezoelectric and other mechanisms. a) A piezoelectric-magnetic composite as magnetic field and deformation bi-sensor. Reprinted from ref. [77], Copyright (2018) with permission from Elsevier. b) Tri-functional EL device with phosphor-piezoelectric effect. Reprinted with permission from ref. [83], Copyright (2018) with permission from John Wiley & Sons.

2.4. Transistors and Resonators

2.4.1. Transistors

Flexible thin film organic field-effect transistors (OFET)[84,85] have been emerging device structures and have contributed greatly to the development of artificial skins,[86] chemical and biological sensors,[87] radio frequency identification tags (RFID),[88] and light-emitting applications.[89] OFET technology is an ideal platform for flexible multi-functional sensors for physical, chemical and biological sensors.[90] Piezoelectrics as multi-functional materials have the potential to serve as the dielectric layer in OFET to achieve multi-functional operation. While at an early stage, multi-functional sensors based on piezoelectric OFET have been made

of several sub-cells and each cell acts as a single mode sensor.[39,91] For instance, Graz, *et al.*[91] fabricated a flexible bifunctional sensor with two integrated sensing elements based on a composite foil of lead titanate ($PbTiO_3$) nanoparticles embedded in an PVDF-TrFE matrix. Using a sequential and area selective poling process, one composite element can be either piezoelectric and another is pyroelectric for pressure and temperature sensing respectively. The capacitance of PVDF-TrFE can be changed with a "static" force or temperature, and the changes in output are not driven by the piezoelectricity or pyroelectricity of PVDF-TrFE.[92] Based on this capacitance change, Hannah, *et al.* fabricated a multi-functional sensor include PVDF-TrFE capacitor combined with an OFET for static/quasi-static force or temperature, see **Figure 7a**. A pressure sensitivity of ~7.5 pF/N was obtained in the range from 0 to ~0.5 N and temperature sensitivity of ~7 pF/°C in the temperature range of 19 to 47 °C.[92]

In the above discussions, the sensors are able to detect force or temperature at one time. Multimodal piezoelectric OFET sensors can provide simultaneous sensing of both temperature and pressure. For example, an ultrathin multimodal sensor based on organic charge-modulated field effect transistors (OCMFET) was able to discriminate between a simultaneously applied temperature and pressure [93]. The OCMFET is a floating-gate OFET with a bottom-gate/bottom-contact configuration that is biased using a control capacitor. As shown in Figure 7b, the multimodal sensor contains two OCMFETs where one is sensitive to pressure and the other is sensitive to both pressure and temperature. Therefore, it is able to easily discriminate between two stimuli by evaluating the difference between the two signals. Conformability and adhesiveness are of great importance for future flexible electronics as it would not affect the biological structure/signal while monitoring.[94] The thickness of this OCMFET is only 1.2 μm, which can be readily attached to human skin, with a high level of conformability and adherence, as shown in Figure 7b. Tien, *et al.* achieved bimodal sensing of temperature and pressure (or strain) simultaneously using an AC gate bias technique in a PVDF-TrFE/$BaTiO_3$ nanoparticles

composite-based OFET sensor. The platform was directly integrated with both a piezo-pyroelectric gate dielectric and piezo-thermoresistive organic semiconductor channel.[6] The approach greatly reduced the complexity in structural integration, eliminated or minimized signal interferences coupled by strain, significantly reduced the power consumption, and decreased the failure rate in production due to facile integration of FET devices into the circuits. Later, the same group improved the sensor sensitivity using a microstructured pyramid PVDF-TrFE (width=4 µm, distance=4 µm, height=2.5 µm) gate dielectric and pentacene channel layer, see Figure 7c.[7] The sensitivity of the sensor reached 1.02 kPa^{-1} under a static pressure range from 20 to 80 Pa and 0.028 kPa^{-1} under dynamic pressure.[7]

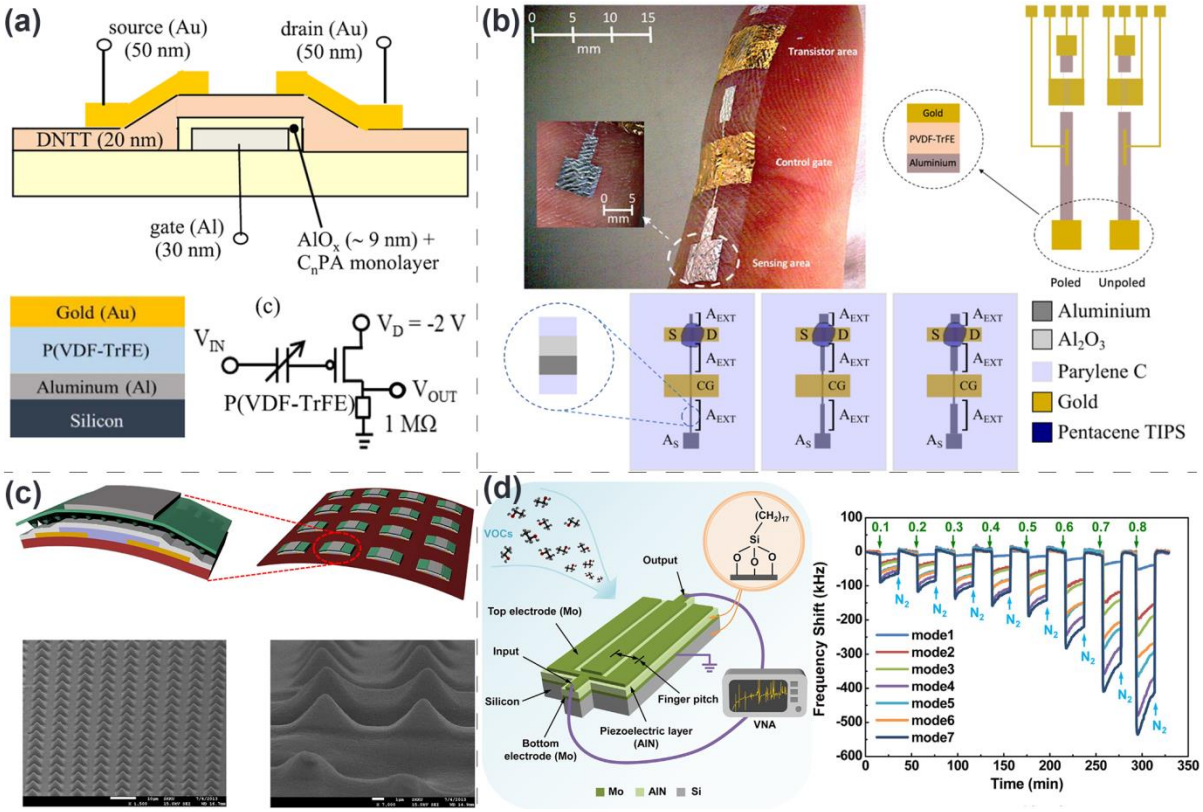

Figure 7. Multi-functional sensors based on piezoelectric transistors and resonators. a) PVDF-TrFE capacitor combined with an OFET for static/quasi-static force or temperature. Reprinted with permission from ref. [92], Copyright (2018) with permission from Elsevier. b) A bimodal temperature and pressure sensor comprised of microstructured PVDF-TrFE as a gate dielectric. Adapted from ref. [93] with permission from Nature Publishing Group , (Copyright 2018). c) An OFET and a transistor array, comprised of microstructured P(VDF-TrFE) as gate dielectric. Reprinted from ref. [7] with permission from Nature Publishing Group , (Copyright 2018). d) Schematic illustration of the multi-mode e-nose and the real-time frequency responses of the

sensor arrays exposed to ethanol vapor with increased gas partial pressures (P/P_0). Reprinted from ref. [26]. Copyright (2018), with permission from Elsevier.

2.4.2. Resonators

One of the unique characteristics of the piezoelectric effect is that it is reversible. The converse piezoelectric effect is when subjected to an electric field, the piezoelectric material exhibits a mechanical deformation. This converse piezoelectric effect has been widely used in high frequency acoustic wave applications particularly resonators, i.e. surface acoustic waves (SAW) resonators and film bulk acoustic wave resonators (FBAR).[95,96] When an alternating electric (AC) electric field is applied, mechanical vibrations are induced and mechanical resonance occurs at an appropriate frequency. Such acoustic wave devices have dominated the frequency control applications in telecommunication industry.[97] Since output frequencies varies with perturbations of wave propagation, the resonators have expanded their applications as novel highly sensitive sensors,[27,98,99] including mechanical,[100,101] chemical and biological sensors.[26,27,102–105] These resonators are fabricated with micro-electro-mechanical system (MEMS) technology and MEMS resonators have the potential for higher level of integration with microelectronics and thus reduce cost, reduce power requirements, and enhance performance and being more functionality.[106]

The mechanism of these sensors is based on changes in the wave propagation speed and drift in the resonant frequency for both SAW and FBAR due to the external stimuli, such as temperature, pressure, and mass loading. A double-layered SAW resonator consists of two series of output changes in temperature and pressure according to the peak values. It has a temperature sensitivity of 4.05 kH/ºC with a sensing range from 25 to 95 ºC and pressure sensitivity of 8.19 kHz/bar for 0-5 bar.[101] Commonly used FBAR devices have two major resonant modes, i.e. longitudinal and shear mode. Based on longitudinal and shear mode resonance, a dual-mode liquid sensor was developed with c-axis tilted piezoelectric aluminum

nitride (AlN) film. [103] The sensitivities of the longitudinal and shear modes to mass loading were 2295 Hz cm^2/ng and 1363 Hz cm^2/ng with mechanical quality factors of 480 and 287, respectively.[103] Manzaneque, *et al.* presented an AlN resonator, vibrating in an out-of-plane mode while immersed in liquid[100] and out-of-plane mode allowed for detecting viscosity and density of the liquid separately. The best resolution of density and viscosity measurement was 1.83×10^{-7} g/ml and 1.74×10^{-5} mPas respectively, see Table 1.[100]

For chemical and biological detection, the surface of the piezoelectric resonator is usually functionalized with specific molecules. The functionalization of the sensing surface enables the surface to selectively bind only to the prescribed set of biomolecules. The molecules adsorb to the functionalized surface allows the change of mass loading and therefore change the resonant frequency of the resonator. In [102], a nanostructure ZnO layer was grown on the top surface of FBAR to form a biosensor. The ZnO was functionalized to selectively immobilize DNA and then hybridized with their fluorescent-tagged complements. The mass sensitivity of this sensor achieved a value up to 1.72×10^3 Hz cm^2/ng. The novel electronic-nose (e-nose) system [107] is specifically used to sense molecules in analogy to the human nose. It can discriminate various volatile organic compounds (VOC) and quantitate compound concentrations and could be developed with a multi-mode FBAR technique.[26,105] Figure 7d shows a schematic of the functionalized e-nose sensor,[26] where the resonator surface was functionalized with gas sensitive trimethoxy (octadecyl) silane (OTES). The frequency responses at multiple resonating modes with mass loadings added on the different regions of the sensor structure, which indicates these values can be used to create a concentration-dependent histogram as VOC's unique "fingerprint" (response spectrum to different compounds). With this "fingerprint", a pattern recognition algorithm could discriminate between the gases. In addition, the imparity distributions of different VOCs on surfaces varies at different positions as different affinity with the target molecules, therefore helped the discrimination of gas vapors.[26] Similar to this work,

an integrated resonator array functionalized with different self-assemble monolayers has been developed to detect five different kinds of VOCs at a trace level.[105] From the adsorption-desorption process of one FBAR array with different concentrations of VOCs, it was noticed that at a constant gas pressure the frequency shifts of different monolayers to a certain type of VOC are discriminative and can be utilized as a "fingerprint".

In addition, there are resonator-based sensors that are not only based on the frequency shift mechanism. For instance, a multi-mode sensing system has been developed that is able to detect glucose concentration change amperometrically and viscometrically by measuring redox reaction, mass changes and viscosity variation.[104] The glucose sensor was developed by integrating electrochemical working electrode with solid-mounted thin film AlN resonator. The electrochemical working electrode shares the resonator's gold electrode layer, which was functionalized with multiple layers of single-walled carbon nanotubes-poly(dimethyldiallylammonium chloride)/glucose oxidase (SWCNT-PDDA/GOD) composite film. The sensor detected the redox current produced by the enzymatic product H_2O_2 and detected the impedance changes of resonator by viscosity change due to glucose concentration.

These miniaturized multi-mode resonators are manufactured based on silicon technology and are easy to integrate or attach to a curved surface. However, they are rigid and have limitation for the soft robotic systems. The flexible resonator can be achieved by wet chemical wafer thinning process[108] or directly fabricate on polymer substrates.[109] Jiang, *et al.* fabricated a high performance free-standing FBAR on PET substrate.[110] The structure was firstly fabricated on a silicon wafer and then transferred onto a PET substrate with the aid of a PDMS stamp and hot embossed air cavities. This method can lead to build future fully flexible multi-functional resonator-based sensors on plastic substrate.

3. Conductive Sensors

The above section discussed flexible piezoelectric-based multi-functional sensors that can simultaneously detect at least two parameters such as pressure, strain, mass, and temperature. The piezoelectric effect plays important role in multi-functional sensors in combination with other sensing mechanisms, such as the piezoresistive effect which corresponds to a change in electrical resistance with stress.

While piezoresistive sensors are flexible, and possesses high sensor performance, they are limited in terms of stretchability. Piezoresistive materials can directly sense static and dynamic stimuli and great effort has been made to develop flexible and stretchable conductive materials. In particular they are useful to develop sensors for measuring biological signals more conveniently and non-invasively and providing safe communications in soft robotic applications. Soft robotics have attracted much attention in recent years due to their safe interaction with objects and human, light weight implementation, low cost and superior biomimetic ability.[28] However, the ability to manipulate fragile and delicate objects with high accuracy remains a challenge for soft robotics. The key challenge for industrial application of soft robotics is the control of soft bodies using materials that integrate sensors, actuators and computation, leading to a soft body which can deliver a desired behavior [111]. Multi-functional stretchable sensors with material compatibility to the underlying soft materials are important to further advance the state of soft robotics. In order to be integrated into a soft robotic system, sensors need to be able to operate under a large deformation or elongation, while not becoming an obstruction to the soft robot's actuation. In this section, we will focus on soft, stretchable conductive sensors based on (i) conductive fabrics, (ii) liquid metals and their applications, including biomedical and robotics applications.

3.1. Conductive Fabric

Conductive fabric based force sensitive sensors have been intensively explored for a variety of applications including biomedical, healthcare, and wearable electronics.[20,112–115] This is a result of their potential to be flexible, conformable and easily attached to any surface [116]. The unique nature of fabrics makes them an ideal vehicle for the design of sensors that are in direct contact with human beings and attached to the surface and skin of robots. In addition, they also possess advantages over conventional materials such as being cost-effective, lightweight, and environmental friendly. Fabrics are hierarchically structured fibrous materials[114] where fibers interlace to form thread, thread gets twisted to form yarn, and yarn can turn into fabric using different weaving and knitting techniques. Generally, the conductive fabric can be manufactured with two types of fibers, i.e. (i) intrinsically conductive fibers; (ii) non-conducting fibers coated with conductive materials. The conductive materials can be either coated on fibers, yarn or fabrics. These will now be discussed.

3.1.1. Intrinsically Conductive Fibers

Intrinsically conductive fibers are often fragile and can be damaged (i) during weaving due to the friction, bending and (ii) after weaving as a result of repeated exposure to tensile and bending strains while wearing or in service. Therefore, a number of conductive fibers have been blended into polyester fibers [117] or embedded in polymer protection layer [118,119] to improve the strength of the fibers. The sensing mechanism of fabrics manufactured from these fibers can be piezoresistive, capacitive or electrostatic.[118] However, most of them are limited to a single functionality, in particular the sensing of pressure or stretch. Recently multi-parameter measurement of pressure and shear force has been realized with an intrinsically conductive fabric.[120] **Figure 8a** shows a pressure-sensitive conductive pile fabric that was knitted by blending a twisted thread made from conductive stainless-steel fibers into polyester. In Figure 8b, it can be seen that under pressure or tension, the cross-sectional area of each conductive thread changes and the number of contact points of stainless-steel fibers inside the yarn

increases, which results in an increase of electrical conductivity. The conductive thread is knitted into a loop shape and when subjected to vertical pressure and shearing force, the knitted conductive thread can be deformed accordingly, as shown in Figure 8c. Therefore, this knitted fabric is able to measure a change in electric resistance due to applied pressure or shear deformation. This pressure-sensitive conductive pile fabric has been placed under the feet to measure the pressure on the sole and the shearing force generated when slipping, as shown in Figure 8d. However, the low restoring force of the fabric does not allow the sensor work under high-load situations, such as walking and running. PDMS has been reported to be an effective cushioning material for pressure-detection sensors inside shoes [121] and for capacitance-type microsensors.[122] Therefore PDMS has been used as protection layer in this sensor to improve its elastic strength and avoid residual deformation, as shown in Figure 8e. Graphene is attracting interest as a high performance and multi-functional material, examples include UV-protection, electroconductivity, photocatalytic, antibacterial, thermally conductive properties, energy storage in flexible supercapacitors, electrodes for batteries, and as a sensing material. Graphene has been fabricated into intrinsically conductive fibers[120] and a multi-functional graphene woven fabric (GWF)[120] has been fabricated by growing graphene on a metal mesh by atmospheric chemical vapor deformation (CVD), followed by removal of the mesh template. The highly conductive GWF has been transferred on PDMS substrate to form a strain sensor but it can be reversible within a relatively low strain range smaller than 5%. Although it is able to achieve electrical conductivity from the continuous path of intrinsically conductive fibers, the fibers do not provide fabrics with adequate strechability. In addition, silicones such as PDMS can protect the fabric but the lack of permeability to air [123] does not provide comfort to people who wear these sensors. Furthermore, human skin can stretch up to 25%[94,124] and some soft robots require a high strechability in excess of 100% strain.[125] Therefore, researchers have explored flexible and stretchable fabrics that are coated with conductive materials.

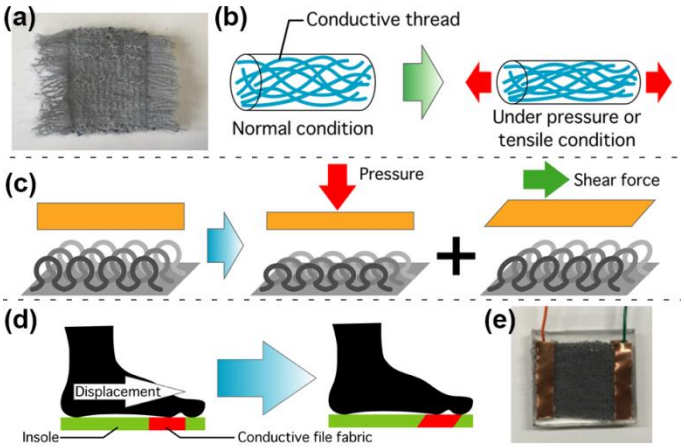

Figure 8. Pressure and shear force measurement principle of pile fabric and a developed PDMS conductive pile fabric. (a) Pressure-sensitive conductive pile fabric, (b) Conductive pile fabric, (c) Detection of vertical pressure & shearing force, (d) Shearing force detection at insole, (e) PDMS conductive pile fabric.

3.1.1. Conductive Materials Coated Fibers

A different approach to form conductive fibers is to coat non-conducting fibers or fabrics with conducting materials. Cotton, PET and polyurethane (PU) fibers have been widely used as non-conducting fibers due to their low cost, durability, and excellent flexibility. A variety of coating methods have been explored,[114] which include screen-printing,[126] dip coating,[127] magnetic sputtering,[128] spray coating,[129] vapor phase polymerization,[130] and direct growth [131] onto non-conducting fibers and then weaving into a conductive fabric. The complete process is simple, cost-effective and controllable. A number of conductive materials have been coated on fibers and it is possible to control the electrical conductivity of the fibers by changing the coating parameters. Conductive materials, including metal nanomaterials, conductive polymers, and carbon-based nano- or micro-structured materials are sensitive to strain, chemicals, gas, and biological signals. Therefore, conducting fabrics can be used to detect mechanical touch, specific environmental or biomedical features, and can also used as an electrothermal heating element.

Metal nanomaterials such as silver and copper nanoparticles can fill the spaces between the cotton nanofibers,[132] and stack together to form a network with high conductivity. A silver/copper coated stretchable fabric acted as an electromagnetic shielding layer and a heating element that was able to help with inhibition of bacteria such as *Staphylococcus aureus* and *Escherichia coli*.[132] In addition, metallic nanoparticles can also form directly on the surface of polymer fibers by converting metallic ions into metallic nanoparticles. Silver precursors have been reduced into silver nanoparticles on poly(styrene-block-butadienstyrene) coated poly(p-phenyleneterephthalamide) fiber.[116] The silver coated single fiber exhibited a significant sensitivity of 0.21 kPa^{-1}, fast response time in the millisecond range and high stability over more than 10000 cycles. The textile-based matrix-type pressure sensor was applied as a human-machine interface to control machines. In another approach, conductive polymer PEDOT:PSS with 5wt% dimethyl sulfoxide (DMSO) was simply spray coated onto PET fabrics [129] layer by layer to form a highly conductive fabric. The high electrical conductivity of this fabric was attributed to the improvement of uniformity, thickness, connectivity and the emergence of PEDOT microcrystals on the multi-ply coatings. This PEDOT:PSS fabric was able to act as a good mobile heater that able to reach 56.2 °C in 100 s under a small bias of 7 V. Ryu, *et al.* developed an intrinsically stretchable multi-functional hollow fiber capable of harvesting mechanical energy and detect strain.[133] The sensor consisted of a piezoelectric P(VDF-TrFE)/PDMS composite layer sandwiched between stretchable piezoresistive electrodes composed of multi-walled carbon nanotubes (MWCNT) and PEDOT:PSS. The combination of MWCNT and PEDOT:PSS acted to decrease the initial resistance of the fiber. The PDMS penetrated into the MWCNT/PEDOT:PSS layer and reversible cracks formed in the MWCNT/PEDOT:PSS when it was stretched and the conductive fiber sensor exhibited a significant gauge factor of 80-177 in the 0-50% strain range, see Table 1.[133]

Among the most commonly used conductive materials, carbon-based nanomaterials, especially nano- and micro-structured graphene, have attracted great attention as multi-functional advanced material for a range of applications since they possess ultra-high electrical conductivity, good electrothermal performance and long-term chemical stability.[134] There are several excellent reviews available on graphene fibers that focus on the production,[135] applications,[136] and device evaluation.[137] Graphene can be synthesized and then coated onto fibers in order to realize different functionalities. Here we review the recent flexible multi-functional sensors fabricated with graphene textile.[120,127,138–140] The microstructure of the fabrics plays an important role in the stretchability of the conductive fabrics. Yuan *et al,* developed an ultra-sensitive 'skin-like' sensor based on a graphene fiber mesh network that was able to monitor pressure, stretch, vibration and bending deformation.[127] In **Figure 9a**, the left PU/polyamide core-spun yarn textile with a spring-like mesh network (SMN) were immersed in chemically converted graphene (CCG) sheet solution for 10 min to form the conductive spring-like GSMN network, right. The GSMN fiber can stretch up to 400% and this high elasticity and elongation can be attributed to the unique spring-like mesh network. Scanning electron microscopy of the GSMN before and after stretching at 50% strain in Figure 9b indicated that the elongation of the GSMN was accommodated by the separation of adjacent polyamide winding fibers or even a change of winding angles, leading to a decrease of the contact area and an increase of the contact resistance. The GSMN, when acting as a pressure sensor, exhibited a high sensitivity of 72 kPa^{-1}, see Figure 9c, and could detect a low pressure of 1.38 Pa induced by a drop of water. It could be further attached on the human body for physiological signal monitoring, such as pulse recording, as shown in Figure 9c.[127]

Other carbon-based materials can be introduced to enhance the performance of graphene. A sandwich-structured conductive natural wool can simultaneously function as a wearable, stretchable and sensitive strain sensor and also as a wearable heater by immersing natural wool

in hybridized graphene nanoplatelets (GNPs) and carbon black (CB) particles mixture suspension.[140] The hybrid of GNPs and CB particles firmly adhered to the surfaces of the cotton/wool fabrics and their single fibers via mechanical interlocking and strong hydrogen bonding. Therefore, this graphene cotton strain sensor possessed a high gauge factor of 20.4, see Table 1, and negligible hysteresis in terms of the response of the strain sensors when subjected up to 50% of strain. The sensors could detect various human movements and sound waves, making them suitable for human−machine interaction electronics. In addition, with a low range of input power, the sensor could be heated up to 103°C and showed excellent electrothermal performance under an applied tensile strain up to 50%.[140]

In addition to graphene, other materials such as ZnO,[131] carbon nanotubes (CNTs) [126] and other piezoresistive materials have been utilized to develop high performance conductive fabrics. In Gao's work, [126] a CNTs/PU conductive paste was screen-printed onto nylon fabric and then covered with a positive triboelectric silk fabric layer to form a single-electrode mode [141] self-powered touch/gesture triboelectric sensors. Human skin acted as negative triboelectric layer for intelligent human-machine interaction, such as to enable access to software on a computer. This CNT based textile had a high conductivity of 0.2 kΩ/sq, high air permeability of 88.2 mm/s and a pressure sensitivity of 0.048 kPa^{-1} at a range of 0 to 110 kPa. It can also be readily incorporated into clothes as a home wireless control device. In addition, this fabric was washable since strong hydrogen bonds were formed between amino groups in PU and carbonyl groups within textiles.[126]

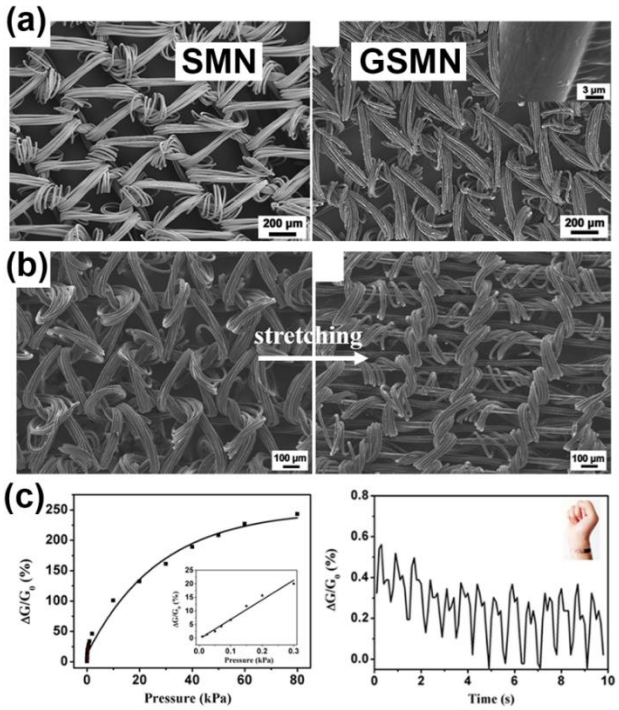

Figure 9. High performance multi-functional skin-like strain sensors based on graphene/spring-like mesh network (SMN)[127] a) SEM image of SMN before and after assembly of CCG sheet. b) SEM images of graphene-coated spring-like mesh network (GSMN) before and after stretching for 50%. c) Conductance variation as a function of pressure ranging from 10 Pa to 80 kPa and Real-time corresponding conductance variation of a GSMN sensor for finger bending and pulse monitoring at human wrist. Reprinted with permission from ref. [127]. Copyright (2018) American Chemical Society.

Since conductive fabric structures are intended to be integrated into clothing and wearable applications, there is a need for the conductivity to remain at the same level after rubbing, stretching or washing. The laundering durability of fabrics has been explored in some studies either by using a standard washing launder machine[139], vigorously stirring in water [29,142] or using a standard detergent according to the ISO 105/C01.[132] Due to the strong adhesion between the conductive materials and fabrics, these conductive fabrics presented only a small loss in electrical conductivity after being sujected to laundering cycles. Kim, *et al.*[142] developed a high durability and waterproofing conductive fabric glove to detect human motion. Cotton fabric was repeatedly immersed into a hybrid solution of reduced graphene oxide and single-wall carbon nanotubes (rGO/SWCNT) for five times. The SWCNTs were bridged in the rGO-coated fabrics, forming random networks with constant nano-scale gaps. This structure

improved the physical contact of adjacent materials and thus enhanced the electrical conductivity. A 100,000 cycle bending test at an extremely small bending radius of 3.5mm suggested that the SWCNTs can also improve the stability of the device and moreover, the rGO/SWCNT fabric device exhibited excellent water resistant properties after 10 washing tests due to its hydrophobic nature. [142] However, there are some conductive fabrics that cannot survive the laundering test at high temperature. For example, in [119] the silicone encapsulation layer on conductive fibers became discolored and started flaking off after a washing cycle at 60 °C.

Rather than coating a fiber or fabric with conducting materials, a novel conductive liquid metal-based microfiber has been developed by Yu and coworkers [29] for force sensing, strain measurements and pulse recording. An elastomeric microtublar structure has been developed by dip-coating a thin metal wire or cotton thread into uncured PDMS and then removing the wire or thread. The liquid metallic alloy, eutectic gallium indium, was then injected into the PDMS elastomeric microtublar structure to form a conductive microfiber. The conductive fiber could be stretched up to 120% and sustained no deterioration in electrical conductivity and functionality after repeated washing. In addition, the material can be woven into a fabric glove to obtain physiological measurement from the wrist, elbow pit, neck and foot instep.[29] Since the intrinsic soft characteristics, liquid metals have also been intensively used as electrodes and sensing elements in soft robotics to ensure safe communication with human beings.[143,144]

3.2. Liquid Metals

3.2.1. Material of Liquid Metal

Soft robots need to work with human beings closely, which requires that the material of the robotic system will not harm the human body. While mercury is a highly toxic liquid metal,

gallium-based liquid metals are practical candidates to develop soft and stretchable sensors with the following considerations:

(i) Low toxicity and ease to use, since gallium has no vapor pressure at room temperature and can be handled without a special requirement of preventing chemical hazards.[145]

(ii) Very high deformability and good electrical conductivity since the deformation limits of liquid metals are only determined by the mechanical properties of the encasing materials[146] and can maintain a high electrical conductivity (3×10^4 S cm^{-1}[147]) up to 1000% stain.[148]

(iii) Material compatibility to soft materials, since the underling material of most soft robots is polymeric and it is important that the liquid metal will not prevent the curing process of the soft materials or have a chemical reaction with the soft materials.

With the above excellent characteristics, much research has been carried out using gallium-based liquid metals to develop sensors for soft robotics. However, it is worth noting that poor adhesion between the liquid metal and the elastic encasing materials remains a challenge. Other common problems include the separation of the liquid metal from the connected electrodes for data acquisition, and the unrecoverable deformation of microchannels.

3.2.2. Fabriaction Methods

The fabrication methods of soft sensors based on a liquid metal can be divided into four categories: injection, lithography, subtractive, and additive methods.[149] In the spectrum of multi-functional soft and stretchable sensors, injection is most widely used fabrication method. Generally, this method contains two major steps: (i) fabrication of a microchannel in an encasing material where a 3D printed sensor mold and lithography are the most commonly used method to create sensing element. (ii) injection of the liquid metal which has a low viscosity (two times of water[150]), making it possible to be injected into multi-layer microchannels to

fabricate multi-functional sensors. This method has been applied to develop many liquid metal based sensors, however, most can only detect a single input,[151] or they are able to detect multiple inputs but cannot decouple them.[146]. The challenge is a result of the underlying principle of using a liquid metal filled microchannel as a sensing element. The sensor's measurement change is a result of its geometrical changes and it is essential to design a novel sensor structure to decouple multiple-inputs.

Park *et al*.[152] reported one of the first attempts to use liquid metal to fabricate a multi-functional sensor, which has the ability to measure strain (in the direction of *x-axis and y-axis*) and pressure *(*in the direction of *z-axis),* for soft artificial skin applications. The system consisted of three sensor layers with embedded microchannels which were connected to the completed final sensing element. Each of the three sensor layers corresponded to one measurement type: layer 1 for *x-axis* strain, layer 2 for *y-axis* strain and layer 3 for *z-axis* pressure. The gauge factors for *x*- and *y-axis* can be found in Table 1. The sensor was able to maintain its linearity up to 100% of strain and could detect a pressure between 15 to 40kPa. The proposed multi-functional sensor failed when the strain was in excess of 250%. The failure was firstly observed at the wire connection site where the material hardness transferred from soft material to rigid material.

Using a force-post embedded into a soft material, as indicated in the figure, Daniel *et al*. developed a soft sensor which could detect a normal force and in-plane forces in two axes, see **Figure 10a**.[30] The force post was used to increase the sensitivity of the sensor and a special microchannel shape was chosen to differentiate the direction and magnitude of the force. The accuracy of the sensor could be increased with a larger number of channels, but at the cost of spatial complexity. Figure 10b shows the fabrication process of the multi-axis sensor based on the method of injection. Sensor molds were 3D printed and the encasing material was Ecoflex since this is one of the most popular encasing materials for making soft and stretchable sensors. In addition to Ecoflex's superior stretchability (break at 1000% elongation for Ecoflex 5), the

good adhesive characteristics of the material make liquid Ecoflex a perfect binding agent to bond multiple layers into a whole part. This design failed when the strain was over 180%. Edward *et al.* [31] presented their work on a multi-mode strain and curvature sensors, as shown in Figure 10c. There were two strain gauges placed back-to-back with a stress concentrator features located in the middle of the whole element. As a result, the sensor was able to differentiate strain, positive curvature and negative curvature. PDMS was used as the encasing material to ensure the softness, flatness and transparence. Lightography was used to fabricate the sensor, resulting in a sensing element of nine layers of silicone elastomer and two different liquid metals filled microchannel structure, as shown in Figure 10d. A low yield rate of the overall system was reported, and over 50% of strain can lead to the failure of the sensor.

The development of multi-functional soft and stretchable sensors based on liquid metals remains challenging due to a lack of a suitable manufacturing method. The rapid advances in 3D printing can be a practical solution to this issue, which can provide a simple, fast, and accurate design and fabrication process.

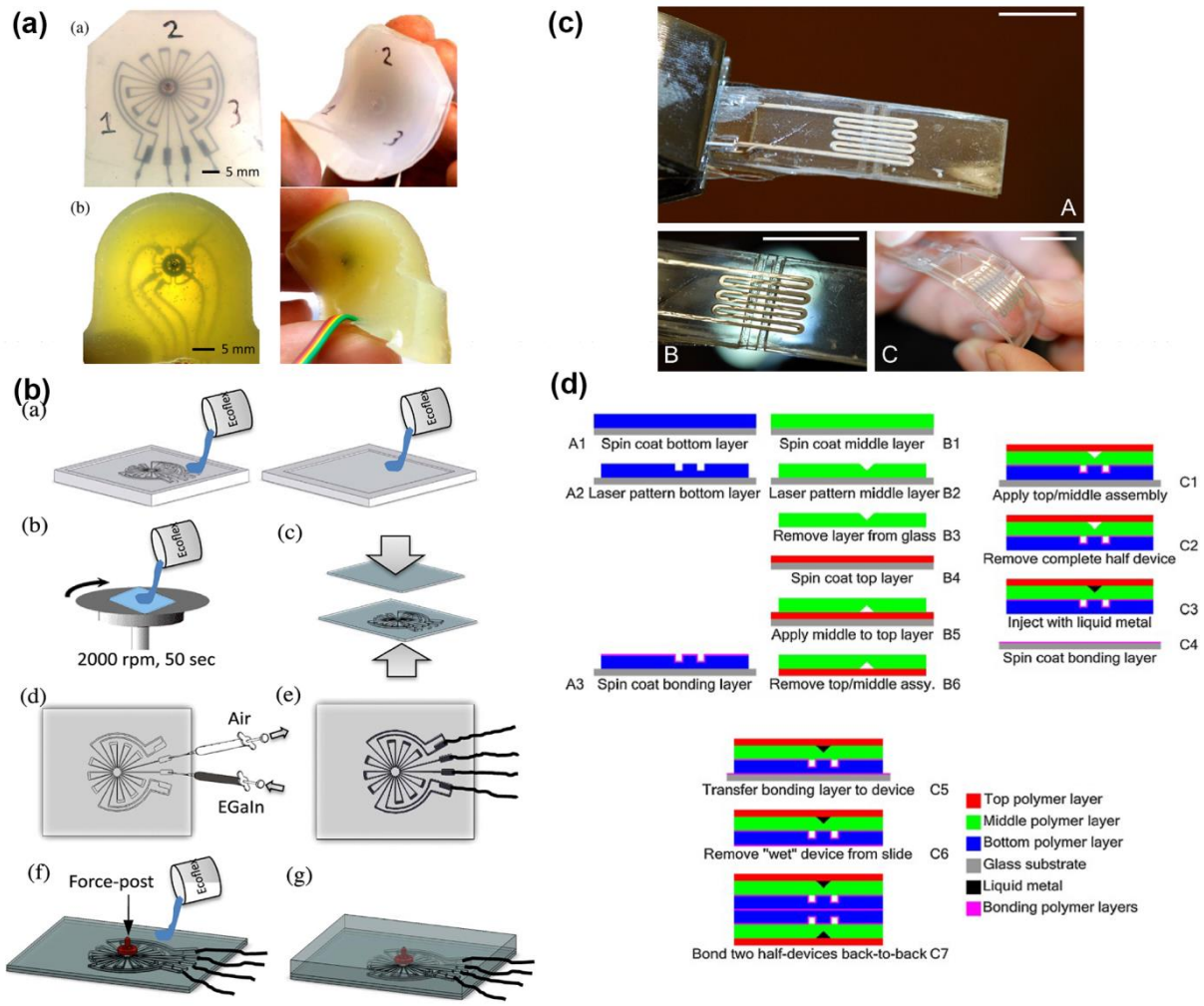

Figure 10. Multi-functional sensors based on liquid metals. (a) Image of a soft multi-axis sensor which can detect normal force and shear force [30]. (b) Sensor fabrication process based on injection [30]. © 2013 IEEE. Reprinted, with permission, from ref. [30] (c) Image of a multi-mode strain and curvature sensor [31]. (d) Sensor fabrication process based on lithography [31]. Reprinted from ref. [31], Copyright (2017) with permission from Elsevier.

4. Optical Sensors with Organic Materials

Electrical sensors such as piezoelectric sensors and conductive paste sensors are continuing to be at the forefront of wearable devices and soft robotics. Such devices offer the most simple and promising way for measuring the deformation of materials by stretching and bending.[153–155] Recently, alternative advanced approaches have been proposed that are based on optically-detectable sensing technology, i.e. optical sensors, for realizing flexible and stretchable sensors. This method provides significant potential for the fine measurement of three-dimensional (3D), complex deformation of soft robots without any influence on their intrinsic characteristics since

light has remote and precise influence, and high spatio-temporally resolution with rapid responsiveness. This means that light does not require any external connections, such as electrodes, for monitoring a materials' deformation. This allows the development of non-invasive, contactless, and flexible sensors. The key to achieve an optical sensor is the development of a novel materials system with high opto-mechanical responsiveness in terms of a change in optical properties in response to deformation.

In nature, there exists abundant examples which could be exploited for the development of future flexible optical sensors.[156–158] As an active and flexible color-changing system, animals such as the chameleon[159] and cephalopods[160] are able to tune the color of their skins autonomously and repeatedly in response to an external environment. This color change is due to light–matter interactions, e.g. transmission, absorption, diffraction, reflection, and luminescence.[161] All phenomena with regard to the origin of color arises from the interaction between electromagnetic waves of light and vibration of electrons in the medium where light passes through. For example, the incident light absorbed by a medium (absorption) excites the electrons to a higher energy level that can potentially emit light (luminescence) of an appropriate wavelength that corresponds to the energy gap. On the other hand, when the material has a periodic distribution of refractive index, which is directly related to the electron density, the materials exhibit the phenomena of diffraction and/or reflection.

Inspired by the unique stimuli-responsive color change in biological systems, a number of researchers have succeeded in achieving a variety of man-made materials that change color after being subjected to mechanical deformation.[162,163] These materials are able to act as a strain sensor for detecting deformation using light. We will explain in detail later in the review how two of the most sophisticated principles in achieving optical sensors are based on reflection or luminescence, and can be classified into three groups depending on how light interacts with

matter: these include photonic crystals, cholesteric liquid crystals, and mechano-chromic materials. In this section, we will introduce each material system by outlining the general mechanism, and present new trends in optical sensing systems before presenting future perspectives.

4.1. Photonic Crystals

Photonic crystals that have a spatially periodic refractive-index distribution at the nanoscale can exhibit a bright color.[164–166] The color corresponds to the reflection of light in the periodic medium that generates a photonic band gap (stop-band), enabling control of light propagation at the wavelength matched with the periodicity of the material. This interesting phenomenon has been pioneered by John[164] and Yablonovitch[165] in the late 1980s where they initially demonstrated one-dimensional (1D) photonic crystals. Motivated by this work, a variety of other photonic crystals with 1- to 3-D periodic structures have been proposed, and has achieved remarkable maturity in the generation of advanced photonic applications such as lasers, waveguides, optical switches, energy harvestings, and sensors.[163,167] Commonly, many state-of-the-art photonic crystals have been fabricated through a "top-down" process including vapor deposition and semiconductor processing of lithography with inorganic materials.[168–170] Although these practical methods are the most commonly used processes for the fabrication of photonic crystals, these principally require significantly hard conditions of high temperature, high vacuum, high processing costs and long production time. There are also challenges in reducing the size of the periodicity for wavelengths less than visible light. Alternatively, the fabrication of photonic structures using a "bottom-up" process have attracted significant attention due to its low cost with a potential to generate a much smaller-periodic structure matched with the UV/Vis wavelength regions. One example of a simple method was firstly proposed by Sanders in 1964 where colloidal mono-dispersed nanoparticles led to self-assembly of the particles into a close-packed array with a 3D opal structure, as shown in **Figure**

11.[171] When the opal structure was back-filled with soft materials such as flexible, transparent polymers or gels, this is inverse opal structure can easily change its shape under external stimuli. In such opal-structured photonic crystals, the reflection of light is ruled by Bragg's law and can be described in Equation 10;

$$\lambda_{max} = 2\sqrt{\frac{2}{3}}d\sqrt{\sum_i n_i^2 \phi_i - \sin^2\theta} \quad (10)$$

where λ_{max} (nm) represents the reflection peak wavelength, d (nm) the size of the hole of opal-structure, n_i the each refractive index of components, ϕ_i the each volume fraction, and θ the incident angle of light. This means that the reflection peak wavelength has a proportional connection with the periodicity, and thus one can control the color of materials merely by tuning the periodicity in broad regions from UV to infrared (IR) light. Since the soft materials can change the shape under external stimuli of heat, chemical treatment, mechanical stress or electric filed, the photonic crystals based on a bottom-up process can exhibit multi-tunability of its optical properties. This class of photonic crystals termed a "tunable photonic crystal", and the concept was firstly proposed by Asher *et al*.[172]

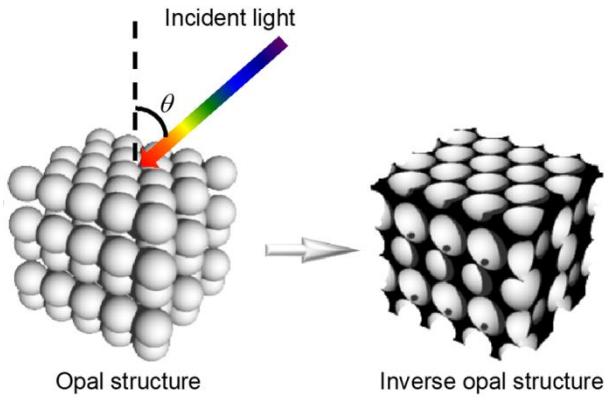

Figure 11. Schematic of the opal and the inverse opal structure fabricated through the bottom-up process where the nanoparticles cause self-assembly into the 3D structure.

After this pioneering work, tunable photonic crystals where formed that were no longer restricted to 3D opal structures; this included the development of 1D lamellae or 2D hexagonally-packed cylinders structures using colloidal nanoparticles, polymer blends, block

copolymers, and gels.[173] Recently, Thomas *et al.* reported a photonic gel of hydrophobic–hydrophilic block-copolymers with 1D periodic lamellar structure that reversely exhibited an exceptionally large stop-band tunability across the UV–Vis and near-IR regions (λ_{max} = 350–1,600 nm) under chemical stimuli; this is in contrast to a conventional system using a 3D opal structure of colloidal particles where the stop-band tunability is only a few hundreds of nm.[174] In this work, the block-copolymer contained units of both a non-swelling glassy block layers and polyelectrolyte block gel layers. By swelling the gel with NH_4Cl aqueous solvent, the gel changed both the spacing and refractive index of layers and the degree of change depended on the concentration of ions; thus, the stop-band position was easily tuned. Shortly after, a variety of photonic gels with broad stop-band tunability have been studied,[173] but there remains a challenge regarding the response time that can take from several seconds to a period of hours. For a detailed discussion on such systems and the mechanisms of tunable photonic crystal the reader is referred to a number of comprehensive reviews.[167,173,175]

To date, a new bio-inspired strategy for achieving tunable photonic gels with ultrafast-response and large stop-band tunability in response to mechanical stimuli was proposed by Yue *et al.* and is shown in **Figure 12a**.[176] They employed chemically crosslinked hydrogels that is a layered system with both bilayer domains of a rigid homo-polymerized poly(dodecyl glyceryl itaconate) and a soft, chemically crosslinked hydrogel layer of hydrolyzed polyacrylamide hydrogel. In this system, the rigid bilayer acts as reflective platelets that not only selectively diffracts visible light by interference but also reinforces the soft gel network, resulting in a mechanically stable material. Thanks to the sophisticated material design, the hydrogel can deform as a quasi-elastic material, enabling an ultra-fast response time (~0.1 ms) even under a small mechanical stress in the order of kilo Pascals, and they demonstrated the ultra-fast mechanical sensing application. Firstly, the gel was subjected to step-wise compression-relaxations under a glass, and then the red-colored gel exhibited a full spectrum color change

($\Delta\lambda_{max}$ ~ 300 nm) with a gradient of color depending on the applied stress field gradient. Furthermore, they designed a ballistic test to determine the response when the gel is subjected to high-velocity impacts. Figure 12c shows a schematic of this experiment where an air gun fired 5-mm diameter plastic spheres at a rubber film in front of the gel, and the color change arising from the deformation was recorded by a high-speed camera with a time resolution of 0.1 ms (Figure 12d). This demonstration clearly showed that that the response time of color switching is about 0.1ms. Furthermore, the fatigue resistance and repeatability of the gel were evaluated, and then they found that such mechano-chromic switching behavior can be repeated for more than 10,000 times without any optical degradation. Such an ultra-fast and robust tunable photonic crystal would be a promising material for quantitatively detecting mechanical deformation and applicable as an optical strain sensor.

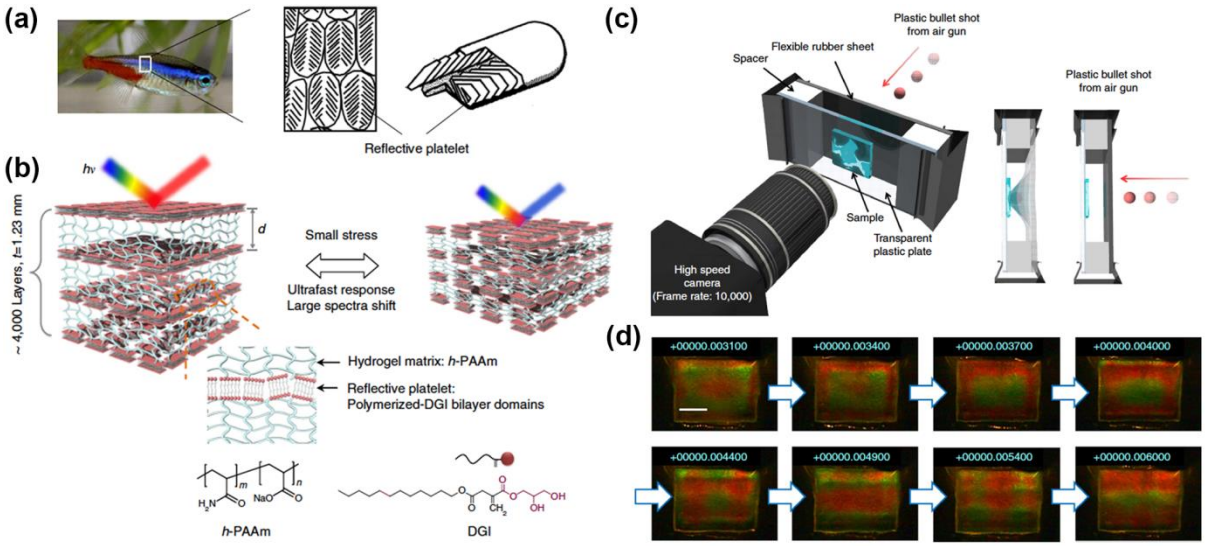

Figure 12. Schematic of bio-inspired photonic hydrogel with ultrafast responsiveness and full-spectrum color tuning. (a) Image of a tropical fish neon tetra with a precise photonic structure, and (b) of the developed photonic hydrogel. The rigid bilayer has a distance of 150-250 nm that selectively reflect visible light. (c) Experimental setup for the ballistic impact test where the gel placed in the center of a transparent plastic plate was struck by a plastic sphere with five-millimeter diameter fired against the gel by an air gun. The deformation due to the impact of the sphere on the sample was detected by color change with high-speed camera. Scale bar, 10 mm. Reproduced with permission.[176] Copyright 2014, Nature Publishing Group.

Recently, another interesting trend for optically detecting a mechanical stress or strain has been reported by Shishido *et al*., along with a number of groups working on this new system.[177–179] In contrast to the advanced photonic crystals, they used the simplest type of classical photonic crystals as the diffraction grating to diffract incident light. The periodicity of the materials' structure has no need to be at the nanometer scale but can be at the micrometer scale, which improves the ease of fabrication, even when using top-down process. They employed low-modulus, amorphous PDMS that can be adhered on any flat substrate and deform in response to the shape change of the substrate. By inscribing the diffraction grating structure on the surface of the PDMS attached to a commercially available poly(ethylene naphthalate) film, they succeeded to remotely monitor the diffraction angles of an incident probe laser beam when the film was bent and were able to quantitatively measure the surface strain. The present method, termed "surface-labeled grating", provides a facile way to optically measure a mechanical strain merely by attaching a PDMS-based external label over any material, with potential to obtain spatial strain mapping.

4.2. Cholesteric Liquid Crystals

Since the first discovery of cholesteric liquid crystals (CLCs) in 1888, CLCs have attracted significant attention as a new class of 1D photonic crystals that is self-assembled into the material with a molecularly controlled refractive-index distribution at the nanoscale.[180] CLCs have helically-twisted molecular orientation where the helical axis is perpendicular to the local homogeneous orientation, as shown in **Figure 13a**. This local orientation is the same as the one of the most common orientational state of the nematic liquid crystal phase. In a nematic liquid crystal phase, anisotropic molecules that are typically rod-like liquid crystals and align homogeneously along one direction termed "director", and thus the nematic liquid crystals have 1D anisotropic refractive index along the director. This is birefringence, where $\Delta n = n_e - n_o$; n_e is the refractive index along the long axis of molecules, and n_o is along short axis. By adding a

small amount of a chiral molecule into a nematic liquid crystals, the director becomes a helically-twisted structure to spontaneously form a CLC phase. Since each layer has the directional order, the CLCs acts as a multi-layer system, such as the periodic structure of a 1D photonic crystal. Therefore, CLCs are able to reflect incident light due to Bragg's law, and the reflection peak wavelength of the CLCs corresponds to when an angle of the incident light is normal to each layer. This can be explained by the following Equation 11:

$$\lambda_{peak} = n_{ave} \cdot P \tag{11}$$

where P is the helical pitch of the orientational structure of CLCs, and n_{ave} (= $(n_e+n_o)/2$) is the average of the refractive indices. Since the liquid crystals intrinsically has two different refractive indices, the reflection light should become broadened depending on Δn. Therefore, the material exhibits a broad band reflection ($\Delta\lambda$; typically ~50 nm) along with the Δn as shown in the Equation 12:

$$\Delta\lambda = \Delta n \cdot P \tag{12}$$

According with this relationship, one can make the reflection wavelength drastically broadened simply by controlling Δn and/or the pitch gradation. This broadening phenomenon has not been achieved with conventional photonic crystals due to its intrinsically precise structure. By making the full of this advantage of CLCs, Broer *et al*. fabricated a wide-band reflection monolith material.[181] They employed a molecular diffusion during polymerization, and induced a concentration gradation of a chiral molecules along the thickness direction. Thus, the polymerized materials had a helical pitch gradation along the direction enabling to reflect a wide-band reflection of $\Delta\lambda$ ~300 nm. It should be noted that this interesting optical property in a monolith material is only achievable by using CLC systems.

Another significant difference between CLCs and the aforementioned photonic crystals is a result of the helically-twisted molecular orientation of CLCs, which is the origin of a unique optical phenomenon, called "selective reflection". Circularly polarized light passing through

the CLCs, where the wavelength and the handedness match with the pitch of helical structure of CLCs can be reflected, and thus CLCs can act as a filter or a reflector of circularly polarized light. When a reflection from conventional photonic crystals is detected, the reflected light does not have any polarization, so that it is difficult to distinguish a signal of a reflected light from background noise. On the other hand, when CLCs are employed, the signal-to-noise ratio can be drastically increased merely by introducing a detector that selectively interacts with circularly polarized light. This is a favorable feature for the use of CLCs as the optical sensor.

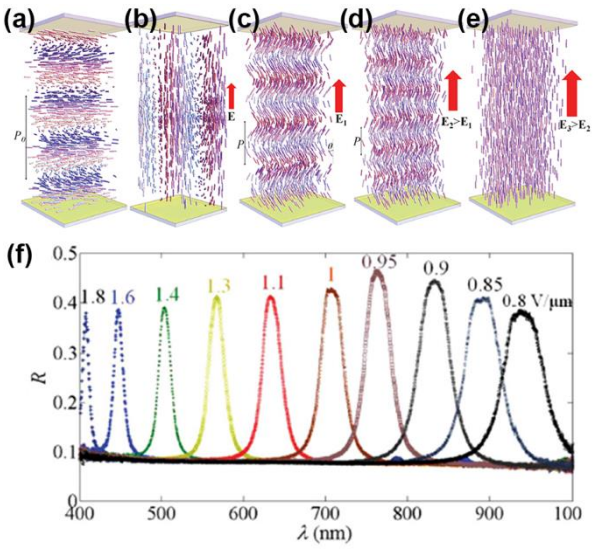

Figure 13. (a-e) Schematic of the local directors (rod-shaped) in cholesteric liquid crystal with right-handedness in a planer cell where the upper and lower plate is coated with electrodes. From (a) to (e), vertical electric field **E** is imposed with the value of 0, sufficiently strong realigning the cholesteric axis perpendicularly to itself, $\mathbf{E}_1$, $\mathbf{E}_2$, $\mathbf{E}_3$ ($\mathbf{E}_1 < \mathbf{E}_2 < \mathbf{E}_3$), respectively. As the field increases, the helical structure becomes tilted and the pitch increases. (f) Selective light reflection spectra of the developed CLC for different amplitudes of the electric field, shown underneath the spectra in V μm^{-1} units. Reproduced with permission.[182] Copyright 2015, WILEY-VCH.

Liquid crystals, sometimes called a “fourth” sate of matter, can have thermotropic properties between the crystalline state (molecular orientation) and isotropic-liquid state (fluidity). The fluidity intrinsically arising from liquid crystals make CLCs highly sensitive to a variety of external stimuli (e.g. light, electric field, pH, or temperature) which changes their orientation order as well as the optical properties. In recent decades, this unique and attractive optical

property has been widely explored, and today CLCs are applied to a number of applications with multi-responsiveness to external stimuli for developing next-generation displays, smart windows, lasers, actuators, and sensors.[180,182–186] One example is shown in **Figure 13**.[182] Lavrentovich *et al*. have developed an electrically responsive CLC with both extraordinary broad tunability of reflective wavelength from UV, visible to IR regions even under low electric fields of a few V μm^{-1}, along with stability over a broad temperature range. Such stability is important for arbitrary tuning and/or sensing of optical properties without any effect of temperature.

A next step for making an optical strain (mechanical) sensor technically feasible would be the generation of mechanically responsive CLCs. Recently, this aim has been achieved by using polymeric liquid crystal polymers, elastomers, polymer networks, and gels that are classified corresponding to to their chemical structure (e.g. chemical composition, crosslinking ratio) that affect mechanical properties such as stiffness, flexibility, and durability. Among such polymeric materials, liquid crystal elastomers are the most favorable for the manifestation of mechanical responsiveness because they can significantly change their shape while maintaining a high mechanical performance.[187] Indeed, there are numerous examples of the fabrication of CLC elastomers (CLCE), which have been applied to various mechanically responsive photonic applications. One of the most simple and easiest procedure for the fabrication of a CLCE is in-situ polymerization of low-molecular weight liquid crystals, where molecular alignment is initially precisely controlled. Such CLCEs show not only a large change of their shape (over 100% strain) under a small mechanical stress, but also recovers it original shape after removing the external force. This shape-changing process with almost zero stress is known as “soft elasticity”, arising from the reorientation of director of the liquid crystals along the applied stress.

The fascinating properties of CLCEs have attracted much attention for developing a family of opto-mechanical applications such as mechanically tunable lasers and strain sensors. After the first experimental demonstration of lasing where an emissive dye were doped in a CLC and lasing occurred at the wavelength of the photonic band-gap,[188] Finkelmann and co-workers presented the dye-doped CLCEs that acted as mirrorless lasers with the mechanical tunability of laser emission wavelength.[189] They synthesized CLCEs with the in-plane molecular alignment having a helical axis along the thickness direction. After applying a mechanical strain onto the CLCE, they succeeded in tuning the lasing wavelength (~50 nm). By application of the stress to the sample film, the film was thinned and simultaneously the helical pitch was shortened. As highlighted above, the relationship between the helical pitch and the reflection wavelength can be described in Equation 12; thus, the lasing wavelength was tuned by mechanical strain. Inspired by this pioneering work, a variety of dyes have been intensively explored for developing a boarded tunability of lasing wavelength. Currently, the lasing wavelength can be tuned across the whole visible region from blue to red (~450 nm to 650 nm).[185] After the discovery of tunable lasing in CLCEs, Shibayev *et al*. in 2010 came up with the novel concept that the mechanical tunability of a photonic band-gap can be used for next-generation mechanical sensors, allowing one to visualize a mechanical stress due to the change of light reflection wavelength.[190] By using a CLCE, they conducted proof-of-concept experiments where the film was subjected to mechanical deformation by stretching, and thus the film exhibited a spontaneous color change which was completely recovered by removing the stretching after a certain duration. This duration was found to have a relationship with the viscosity of the CLCE, so that they proposed a quantitative model of viscoelastic materials. Based on the model, they fully explained both the shape change behavior and color changes. Furthermore, Picot *et al*. presented a flexible, optical strain sensor enabling real-time monitoring of uniaxial deformation in CLCEs films, and this strain sensor enables the detection of strain by the naked eye.[191]

Compared with conventional photonic crystals initially described in this section, CLCEs have the advantage of a facile fabrication process since they can be fabricated in a single-step using a self-assembly process. Thus, CLCEs provide a pathway for achieving optical strain sensors that can be attached to any materials' surface. By making the best use of this feature, a variety of facile processing methods of CLCEs have been proposed.[192,193] Recently, Schenning *et al*. proposed a new material system that is well-adhering, which can easily produce CLCEs including reactive mesogens, crosslinkers and photoinitiators, see **Figure 14**.[192] The transparent mixture was bar-coated over a polycarbonate substrate, and subsequently photopolymerized, resulting in a highly molecularly aligned CLCE that were well adhered to the substrate shown in Figure 14d. Even using such a facile fabrication process, the resultant CLCE could be coated over a polymer substrate and exhibit the properties of photonic crystals with high transparency and reflectance, and thus is highly favorable scaling up as an industrial processes.

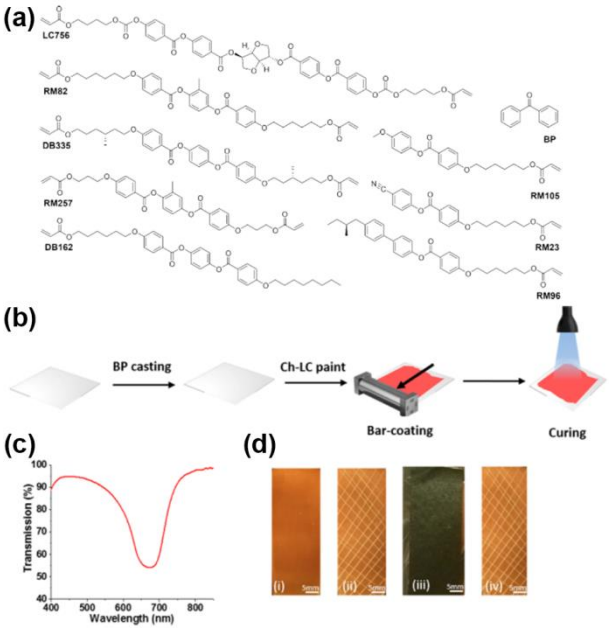

Figure 14. (a) Molecular structures of the chemicals used for the fabrication of CLCE. (b) Schematic for preparation and coating of cholesteric LCs mixture painted by using an facile process of bar-coating technique over a plastic surface. (c) Transmission spectrum of the CLCE coating after the curing process. (d, i-iv) Photograph of a CLCE, the cross-hatch pattern inscribed over the surface of a CLCE before conducting the tape test, a CLCE coating covered

with a Tesa 4651 tape, and adhered coating remaining after the rapid removing the tape, respectively. Reproduced with permission.[191] Copyright 2018, American Chemical Society. <https://pubs.acs.org/doi/abs/10.1021%2Facsami.8b11583>.

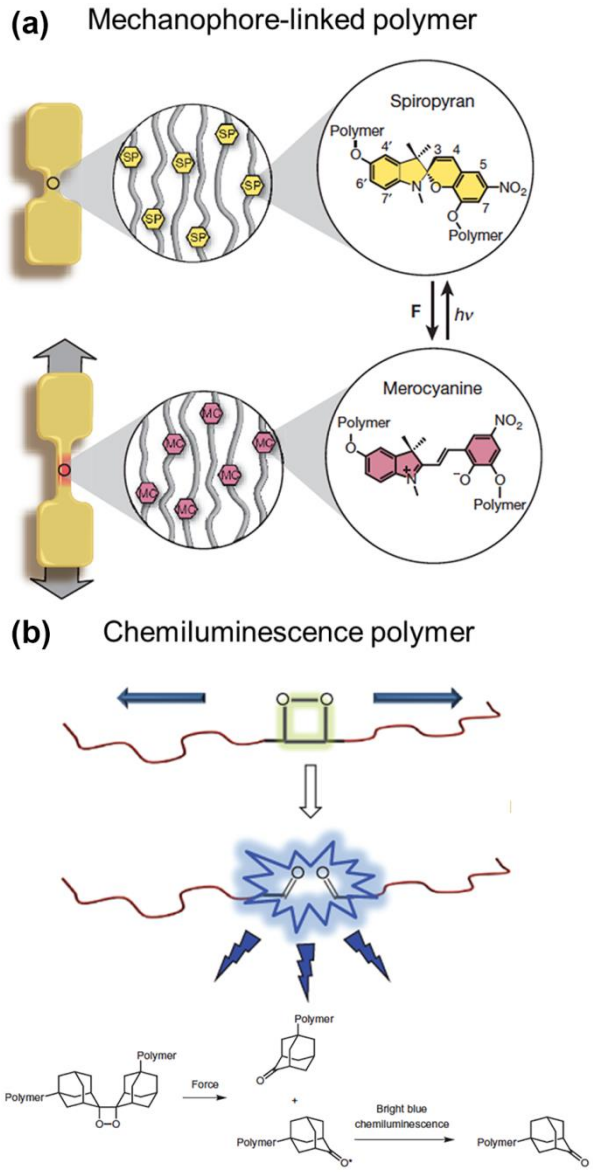

Figure 15. Schematic of mechano-responsive molecules incorporated into a polymer mainchain. (a) Specimens including spiropyran-based mechanophore under application of tensile force caused the color change due to the conversion between the colorless spiropyran and colored merocyanine forms. The color recovers under exposure to visible light. Reproduced with permission.[194] Copyright 2009, Nature Publishing Group. (b) Chemiluminescence polymer with bis(adamantyl) dioxetane induced luminescence under mechanical stress resulting in the ketone product. Reproduced with permission.[195] Copyright 2009, Nature Publishing Group.

4.3. Mechano-chromic Systems

Other potentially fascinating developments that allow one to measure mechanical deformation with extremely high spatial resolution without any external energy source have been

proposed.[196] In a mechano-chromic system, the molecules individually show a color change due to the absorption and/or emission of light in response to the mechanical strain/stress on the materials. The key initial discovery was reported by Scott *et al*. in late 2000 where a polymeric system included a rational unit, a so-called mechanophores, that enabled the material to exhibit mechanically induced changes in color and/or fluorescence.[194,197] They incorporated a mechanophore based on spiropyran derivatives into a center of polymer mainchain as shown in **Figure 15a**. This new material system enables one to visualize the mechanical stress by changing the macroscopic color of the polymer film. In this research, the spiropyran mechanophore changes a molecular structure of the spiro-junction from spiropyran (no strain; yellow color) to merocyanine (under strain; red color), and thus acts as a molecular force sensor within the bulk polymeric system. The advantages of this new visualization systems of mechanical strain are the ability to detect the effect of not only the force, but also damage or pressure applied to the material. Recently, numerous types of mechano-chromic polymers with precisely designed mechanophores have been developed; thus, polymeric systems (e.g. polymers, block-copolymes, supramolecules, etc.) are able to detect a variety of mechanical stimuli, such as stretching, grinding, pressing, swelling or freezing, through the multicolor changes.[196,198]

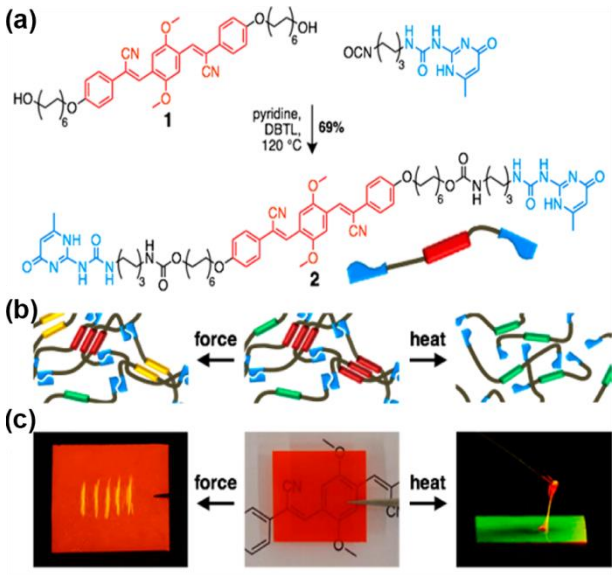

Figure 16. (a) Chemical structures and mechanism of color change due to the formation of supramolecular polymer. (b) Schematic of assemblies under external stimuli of mechanical force or heat. (c) Films fabricated from the present supramolecule, mechano- (left) and thermos-responsive (right) luminescent behavior under illumination with 365 nm UV light. The fluorescence changes from red to yellow upon scratching (left), and to green upon heating at 180 °C. Reproduced with permission.[199] Copyright 2017, American Chemical Society.

Among such advanced mechanophores, light emissive mechanophores, emitting a light in response to mechanical stimuli, have also attracted attention.[196] Sijbesma *et al.* firstly reported a family of such light emissive mechanophores, causing covalent bond scission of a polymer main chain with 1,2-dioxetanes.[195] By imposing a mechanical stress on the polymeric material, a emissive mechanophore of bis(adamantyl)-1,2- dioxetanes resulted into the ketone product with a higher energy state due to bond scission, and then the product is relaxed to the ground state along with the emission of light, as shown in Figure 15b. Thanks to this autoluminescent nature, this material system does not require to use any external excitation light source, which is typically used for conventional mechanophores. Therefore, the autoluminescent enables one to detect the deformation as well as mechanical stress at real-time scales with high spatio-temporal resolution. Unfortunately, this system is intrinsically irreversible due to the use of bond scission and the ability to achieving a reversely detectable mechanophore is highly desirable. In conventional systems based on mechanophores previously reported, the emission is altered depending on the molecular packing structure and/or bond scission of a single molecules embedded in polymers. Thus, it is challenging to realize reversible detection and reveal the direct relationship between the polymer deformation and the change of color and/or fluorescence of mechanophores.

As an alternative approach, Weder *et al*. designed a new mechano-responsive material that uses supramolecular interaction (**Figure 16**).[199] In this system, the mechanophore with both hydrogen bonding and π-π stacking resulted in a supramolecular polymer formed *via* a self-assembly process, and the material reversibly exhibited different colors under mechanical stress

or heat. This new approach allows ones to design various mechano-responsive polymeric systems. Interestingly, a new type of mechanophore has also been proposed by Filonenko and Khusnutdinova where the material system does not require covalence bond scission or a chemical structural change and is shown on **Figure 17**.[200] They employed a family of Cu(I) phosphorescent complexes where the photoluminescence property is remarkably sensitive to the local environment. They incorporated the phosphor into a polymer and subjected it to a mechanical stress, and found that this material dynamically, reversibly changed the phosphorescence intensity depending on the stress due to the structural change of aggregate structure of molecules.

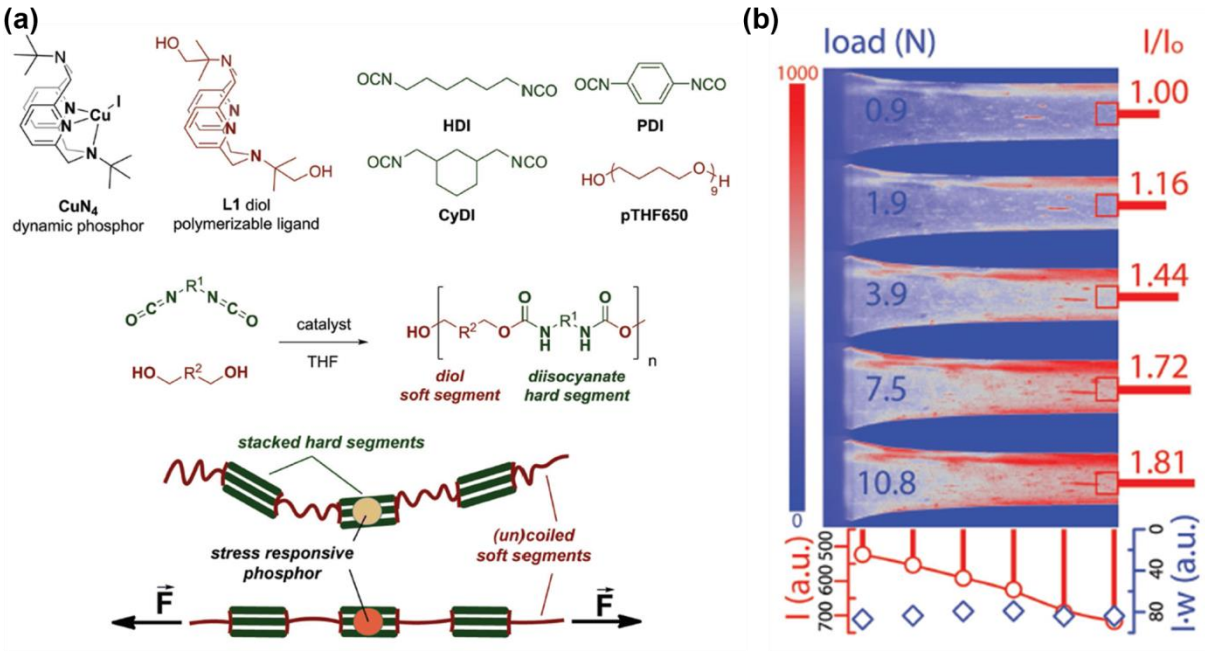

Figure 17. (a) Structures of the building blocks and properties of a new type of materials. The present mechanophore does not require changes to its molecular structure or arrangement and relies fully on suppression of nonradiative relaxation. (b) Optical images of the materials under both applied stress and excitation light at 354 nm, and photoluminescence intensity (measured across the sample elongation direction, red circles) and width-corrected intensity (blue diamonds) distribution along the sample loaded at 10.8 N. Reproduced with permission.[200] Copyright 2017, WILEY-VCH.

Another trend of light emissive strain sensor is using piezoluminescent inorganic materials dispersed in polymeric systems, and recently this has been practically applied for detecting fracture of infrastructures such as industrial plants and buildings. Piezoluminescence is a mechano-luminescence behavior, and they exhibit autoluminescence that is dependent on the

internal piezoelectric field induced by elastic deformation of materials. Thus, such materials offer the opportunity for the development of wireless, nondestructive, facile detection of stress and/or damage of materials. Since the first report of piezoluminescence (elastic mechano-luminescence) by Atari *et al.* in 1982,[201], such materials has attracted attention for use as a practical optical sensor to detecting stress and damage imposed on materials. Recently, Xu *et al.*, one of the leading groups in this field, developed $SrAl_2O_4$:Eu piezoluminescence material embedded in an epoxy resin (a polymeric system), and found that this resin can be used for a non-destructive evaluation method for detecting a crack produced in metals.[202] Furthermore, in 2017, the group presented an efficient, thresholdless red-emitting piezoluminescence system where Pr_3^+ was doped into the well-known piezoelectric matrix, $LiNbO_3$, and demonstrated the stress-sensing performance of this system for practical use in industry.[203] They coated the material over the surface of an aluminum alloy plate, and applied the tensile strain onto the plate. As a result, this material repeatedly exhibited continuous mechano-luminescence with the strain change, and the luminescence intensity was tuned even with very low strain (~1 x 10^{-4} % strain). This is the first development of the piezoluminescence materials detecting very low strain with a potential for achieving high-precision detection and high-resolution imaging. Thus, this new class of material can be applicable for flexible robots by combining with polymeric system, and would pave the way for precise, repeatable microstrain detection.

5. Conclusions and Perspectives

This review has provided a detailed overview of the current state-of-the-art of flexible multi-functional sensors for wearable and robotic applications. Significant progress has been made in the development and advancement of flexible and multi-functional sensors for applications related to healthcare, robotics and biomedical areas; these are application sectors where there is a demand for high sensitivity, accuracy, reproducibility, mechanical flexibility and low cost. Processing routes for the fabrication of such sensors should ideally be compatible with large-

area processing techniques and allow ease of integration into flexible devices and surfaces. The ability to empower robots and future e-skins with high resolution, high sensitivity and rapid response sensing capabilities is of interest to a broad range of applications including wearable healthcare devices, biomedical prosthesis, human-machine interacting robots such as service robots for the elderly and electronic skin to provide a range of diagnostic and monitoring capabilities.

There are a wide range of sensing mechanisms that can be exploited, and many are summarized in Figure 1. This includes piezoelectric, pyroelectric, piezoresistive, triboelectric, magnetoelectric and electro-luminescence effects, with potential for their combination with chemical and biological sensors. For ease of integration and large area production, the use of textiles with multi-functional properties is an attractive solution, including those manufactured from conductive materials, coated textiles and liquid metals. As an alternative to the physical sensors described above, optical sensors have potential to be used as a robotic or e-skin; this included sensory color changes using photonic crystals, liquid crystals, and mechano-chromic effects. The challenge for these exciting materials is to enhance their integration into wearables and robotic applications.

Potential future directions include a greater demonstration of multi-functional sensor systems deployed on robotics or as e-skins, rather than smaller scale sensor demonstrators. There is also potential to use machine learning to optimize sensors response and this may be particularity important for multi-functional sensors which have a wide range complex inputs from a variety of stimuli. The development of low-cost flexible sensors with ultra-low power consumption can also be considered; this can extend the range of applications and tackle the challenges of energy-inefficiency and cost-inefficiency of current flexible sensors. In addition to low power consumption, the development of self-powered sensors that integrate energy generation and

sensing processes together would be of interest as this could eliminate current barriers for current biomedical devices that rely on the powered sensors to monitor the real-time conditions. Sensitivity continues to be of importance, and the fabrication of ultra-sensitive sensors to enable real-time detection of ultra-low pressure (<1 Pa); this may be used for future healthcare devices and highly sensitive e-skin applications. Optical sensing is particularly innovative and attractive, however more effort in required to create flexible and compliant optical sensors for e-skin applications. Printed electronics especially sensors manufactured with 3D printing technology[204,205] have drawn much attention in recent years. It offers significant opportunities to create complex sensor configurations, provides a freedom of custom design, and also can provide direct integration of multi-material into a single sensor. As an extension of 3D printing, 4D printing[206] provides an additional dimensions of transformation over time, which would further provide an innovate approach for the future sensor design and manufacturing. Finally, to provide a robust system, further material innovation is needed to fabricate intelligent multi-functional devices, such as development of multi-functional sensors with self-healing ability to ultimately mimic function of human skin and enables sensors and future robots to work in harsh environment.

Conflict of Interest

The authors declare no conflict of interest.

Acknowledgements

Prof. C. Bowen would like to acknowledge the funding from the European Research council under the European Union's Seventh Framework Programme (FP/2007-2013)/ERC Grant Agreement No. 320963 on Novel Energy Materials, Engineering Science and Integrated Systems (NEMESIS). Dr. M. Xie, Dr. Z. Mingzhu, Dr. Toyoshi, Dr. S. Okada, Prof. O. Tsutsumi, and Prof. Kawamura would like to thank Ritsumeikan Global Innovation Research Organization "Robotics innovation based on advanced materials". Dr. Zhu would like to thank MEXT Kakenhi 17H07255, JSPS, Japan. The authors would also like to acknowledge Prof. M. Makikawa for the helpful suggestions regarding conductive pile fabric in section 3.

Received: ((will be filled in by the editorial staff))
Revised: ((will be filled in by the editorial staff))
Published online: ((will be filled in by the editorial staff))

References

[1] Y. Zang, F. Zhang, C. A. Di, D. Zhu, *Mater. Horizons* **2015**, 140.

[2] J. Tegin, J. Wikander, *Ind. Rob.* **2005**, *32*, 64.

[3] M. L. Hammock, A. Chortos, B. C.-K. C. K. Tee, J. B. H. B.-H. Tok, Z. Bao, *Adv. Mater.* **2013**, *25*, 5997.

[4] G. Schwartz, B. C. K. Tee, J. Mei, A. L. Appleton, D. H. Kim, H. Wang, Z. Bao, *Nat. Commun.* **2013**, 3002.

[5] L. Pan, A. Chortos, G. Yu, Y. Wang, S. Isaacson, R. Allen, Y. Shi, R. Dauskardt, Z. Bao, *Nat. Commun.* **2014**, 3002.

[6] N. T. Tien, S. Jeon, D. Kim, T. Q. Trung, M. Jang, B. Hwang, K. Byun, J. Bae, E. Lee, J. B. Tok, *Adv. Mater.* **2014**, *26*, 796.

[7] D.-I. Kim, T. Q. Trung, B.-U. Hwang, J.-S. Kim, S. Jeon, J. Bae, J.-J. Park, N.-E. Lee, *Sci. Rep.* **2015**, *26*, 12705.

[8] S. Y. Kim, S. Park, H. W. Park, D. H. Park, Y. Jeong, D. H. Kim, *Adv. Mater.* **2015**, *27*, 4178.

[9] B. C. K. Tee, C. Wang, R. Allen, Z. Bao, *Nat. Nanotechnol.* **2012**, *7*, 825.

[10] X. Wang, L. Dong, H. Zhang, R. Yu, C. Pan, Z. L. Wang, *Adv. Sci.* **2015**, *2*, 1500169.

[11] S. C. B. Mannsfeld, B. C. K. Tee, R. M. Stoltenberg, C. V. H. H. Chen, S. Barman, B. V. O. Muir, A. N. Sokolov, C. Reese, Z. Bao, *Nat. Mater.* **2010**, *9*, 859.

[12] T. Q. Trung, N. E. Lee, *Adv. Mater.* **2016**, *28*, 4338.

[13] D. Kang, P. V. Pikhitsa, Y. W. Choi, C. Lee, S. S. Shin, L. Piao, B. Park, K. Y. Suh, T. Il Kim, M. Choi, *Nature* **2014**, *516*, 222.

[14] C. Dagdeviren, Y. Su, P. Joe, R. Yona, Y. Liu, Y. S. Kim, Y. Huang, A. R. Damadoran, J. Xia, L. W. Martin, Y. Huang, J. A. Rogers, *Nat. Commun.* **2014**, 4496.

[15] C. Li, P. M. Wu, L. A. Shutter, R. K. Narayan, *Appl. Phys. Lett.* **2010**, *96*, 053502.

[16] M. C. Yu, M. S. Yu, M. K. Yu, F. Lee, W. H. Huang, *Pediatr. Nephrol.* **2011**, *26*, 233.

[17] Z. Li, Z. L. Wang, *Adv. Mater.* **2011**, *23*, 84.

[18] X. Wang, Y. Gu, Z. Xiong, Z. Cui, T. Zhang, *Adv. Mater.* **2014**, *26*, 1336.

[19] K. A. Cook-Chennault, N. Thambi, A. M. Sastry, *Smart Mater. Struct.* **2008**, *17*, 043001.

[20] M. Stoppa, A. Chiolerio, *Sensors (Switzerland)* **2014**, *14*, 11957.

[21] J. W. Jeong, W. H. Yeo, A. Akhtar, J. J. S. Norton, Y. J. Kwack, S. Li, S. Y. Jung, Y. Su, W. Lee, J. Xia, H. Cheng, Y. Huang, W. S. Choi, T. Bretl, J. A. Rogers, *Adv. Mater.* **2013**, *25*, 6839.

[22] S. H. Nam, P. J. Jeon, S. W. Min, Y. T. Lee, E. Y. Park, S. Im, *Adv. Funct. Mater.* **2014**, *24*, 4413.

[23] J. A. Paradiso, T. Starner, *IEEE Pervasive Comput.* **2005**, *4*, 18.

[24] P. D. Mitcheson, E. M. Yeatman, G. K. Rao, A. S. Holmes, T. C. Green, *Proc. IEEE* **2008**, *96*, 1457.

[25] L. M. Swallow, J. K. Luo, E. Siores, I. Patel, D. Dodds, *Smart Mater. Struct.* **2008**, *17*, 025017.

[26] Y. Zhao, Q. Yang, Y. Chang, H. Qu, W. Pang, H. Zhang, X. Duan, *Sensors Actuators, B Chem.* **2018**, *254*, 1191.

[27] I. Voiculescu, A. N. Nordin, *Biosens. Bioelectron.* **2012**, *33*, 1.

[28] D. Trivedi, C. D. Rahn, W. M. Kier, I. D. Walker, *Appl. Bionics Biomech.* **2008**, *5*, 99.

[29] L. Yu, J. C. Yeo, R. H. Soon, T. Yeo, H. H. Lee, C. T. Lim, *ACS Appl. Mater. Interfaces* **2018**, *10*, 12773.

[30] D. M. Vogt, Y.-L. Park, R. J. Wood, *IEEE Sens. J.* **2013**, *13*, 4056.

[31] E. L. White, J. C. Case, R. K. Kramer, *Sensors Actuators, A Phys.* **2017**, *253*, 188.

[32] A. Grillet, D. Kinet, J. Witt, M. Schukar, K. Krebber, F. Pirotte, A. Depré, *IEEE Sens. J.* **2008**, *8*, 1215.

[33] S. Bauer, S. Bauer-Gogonea, I. Graz, M. Kaltenbrunner, C. Keplinger, R. Schwödiauer,

Adv. Mater. **2014**, *26*, 149.

[34] J. Peirs, J. Clijnen, D. Reynaerts, H. Van Brussel, P. Herijgers, B. Corteville, S. Boone, *Sensors Actuators, A Phys.* **2004**, *115*, 447.

[35] G. Gautschi, in *Piezoelectric Sensorics*, Springer, **2002**, pp. 73–91.

[36] E. F. Crawley, J. De Luis, *AIAA J.* **1987**, *25*, 1373.

[37] D. Damjanovic, *Rep. Prog. Phys* **1998**, *61*, 1267.

[38] C. R. Bowen, H. a. Kim, P. M. Weaver, S. Dunn, *Energy Environ. Sci.* **2014**, *7*, 25.

[39] I. Graz, M. Kaltenbrunner, C. Keplinger, R. Schwödiauer, S. Bauer, S. P. Lacour, S. Wagner, *Appl. Phys. Lett.* **2006**, *89*, 073501.

[40] S. Harada, W. Honda, T. Arie, S. Akita, K. Takei, *ACS Nano* **2014**, *8*, 3921.

[41] B. JAFFE, W. R. COOK, H. JAFFE, in *Piezoelectric Ceram.*, **1971**, pp. 7–21.

[42] S. O. R. Moheimani, A. J. Fleming, *Piezoelectric Transducers for Vibration Control and Damping*, Springer Science & Business Media, **2006**.

[43] Y. Nemirovsky, A. Nemirovsky, P. Muralt, N. Setter, *Sensors Actuators A Phys.* **1996**, *56*, 239.

[44] C. R. Bowen, J. Taylor, E. LeBoulbar, D. Zabek, A. Chauhan, R. Vaish, *Energy Environ. Sci.* **2014**, *7*, 3836.

[45] C. R. Bowen, M. Xie, Y. Zhang, V. Y. Topolov, C. Wan, in *Ferroelectr. Mater. Energy Appl.*, Wiley-VCH Verlag GmbH & Co. KGaA Weinheim, Germany, **2018**, pp. 203–229.

[46] S. B. Lang, *Phys. Today* **2005**, *58*, 31.

[47] F. R. Fan, W. Tang, Z. L. Wang, *Adv. Mater.* **2016**, *28*, 4283.

[48] Q. Zheng, B. Shi, Z. Li, Z. L. Wang, *Adv. Sci.* **2017**, *4*, 1700029.

[49] G. T. Hwang, M. Byun, C. K. Jeong, K. J. Lee, *Adv. Healthc. Mater.* **2015**, *4*, 646.

[50] Z. Lou, L. Li, L. Wang, G. Shen, *Small* **2017**, *13*, 1701791.

[51] T. Huynh, H. Haick, *Adv. Mater.* **2018**, 1802337.

[52] Y. Hu, Z. L. Wang, *Nano Energy* **2014**, *14*, 3.

[53] M. H. Lee, R. Guo, A. S. Bhalla, *J. electroceramics* **1998**, *2*, 229.

[54] M. Xie, Y. Zhang, M. J. Kraśny, C. Bowen, H. Khanbareh, N. Gathercole, *Energy Environ. Sci.* **2018**, *11*, 2919.

[55] Y. Lee, J. Park, S. Cho, Y. E. Shin, H. Lee, J. Kim, J. Myoung, S. Cho, S. Kang, C. Baig, H. Ko, *ACS Nano* **2018**, *12*, 4045.

[56] P. Muralt, R. G. Polcawich, S. Trolier-McKinstry, *MRS Bull.* **2009**, *34*, 658.

[57] K. Maity, D. Mandal, *ACS Appl. Mater. Interfaces* **2018**, *10*, 18257.

[58] G. Zhao, X. Zhang, X. Cui, S. Wang, Z. Liu, L. Deng, A. Qi, X. Qiao, L. Li, C. Pan, Y. Zhang, L. Li, *ACS Appl. Mater. Interfaces* **2018**, *10*, 15855.

[59] D. B. Deutz, N. T. Mascarenhas, J. B. J. Schelen, D. M. de Leeuw, S. van der Zwaag, P. Groen, *Adv. Funct. Mater.* **2017**, *27*, 1700728.

[60] X. Chen, X. Li, J. Shao, N. An, H. Tian, C. Wang, T. Han, L. Wang, B. Lu, *Small* **2017**, *13*, 1604245.

[61] H. Xue, Q. Yang, D. Wang, W. Luo, W. Wang, M. Lin, D. Liang, Q. Luo, *Nano Energy* **2017**, *38*, 147.

[62] H. ATHENSTAEDT, *Nature* **1970**, *228*, 830.

[63] H. Athenstaedt, H. Claussen, D. Schaper, *Science (80-.).* **1982**, *216*, 1018.

[64] S. H. Shin, D. H. Park, J. Y. Jung, M. H. Lee, J. Nah, *ACS Appl. Mater. Interfaces* **2017**, *9*, 9233.

[65] J. S. Lee, K.-Y. Shin, O. J. Cheong, J. H. Kim, J. Jang, *Sci. Rep.* **2015**, *5*, 7887.

[66] M. S. Suen, Y. C. Lin, R. Chen, *Sensors Actuators, A Phys.* **2018**, *269*, 574.

[67] W. Zhang, C. Hou, Y. Li, Q. Zhang, H. Wang, *Nanoscale* **2017**, *9*, 17821.

[68] S. Gupta, L. Lorenzelli, R. Dahiya, in *SENSORS, 2017 IEEE*, IEEE, **2017**, pp. 1–3.

[69] Y. Chen, Y. Zhang, F. Yuan, F. Ding, O. G. Schmidt, *Adv. Electron. Mater.* **2017**, *3*, 1600540.

[70] K. S. Tan, W. C. Gan, T. S. Velayutham, W. H. A. Majid, *Smart Mater. Struct.* **2014**, *47*, 125006.

[71] R. Zhang, B. Jiang, W. Cao, *J. Appl. Phys.* **2001**, *90*, 3471.

[72] G. T. Hwang, H. Park, J. H. Lee, S. Oh, K. Il Park, M. Byun, H. Park, G. Ahn, C. K. Jeong, K. No, H. Kwon, S. G. Lee, B. Joung, K. J. Lee, *Adv. Mater.* **2014**, *26*, 4880.

[73] J. Park, M. Kim, Y. Lee, H. S. Lee, H. Ko, *Sci. Adv.* **2015**, *1*, e1500661.

[74] S. W. Kim, Y. Lee, J. Park, S. Kim, H. Chae, H. Ko, J. J. Kim, *Sensors (Switzerland)* **2018**, *18*, 78.

[75] A. Kimoto, N. Sugitani, S. Fujisaki, *IEEE Sens. J.* **2010**, *10*, 1508.

[76] R. Gonçalves, A. Larrea, M. S. Sebastian, V. Sebastian, P. Martins, S. Lanceros-Mendez, *J. Mater. Chem. C* **2016**, *4*, 10701.

[77] M. Sang, S. Wang, M. Liu, L. Bai, W. Jiang, S. Xuan, X. Gong, *Compos. Sci. Technol.* **2018**, *165*, 31.

[78] Y. K. Mishra, G. Modi, V. Cretu, V. Postica, O. Lupan, T. Reimer, I. Paulowicz, V. Hrkac, W. Benecke, L. Kienle, R. Adelung, *ACS Appl. Mater. Interfaces* **2015**, *7*, 14303.

[79] J. Sun, P. Li, R. Gao, X. Lu, C. Li, Y. Lang, X. Zhang, J. Bian, *Appl. Surf. Sci.* **2018**, *427*, 613.

[80] W. Han, L. Zhang, H. He, H. Liu, L. Xing, X. Xue, *Nanotechnology* **2018**, *29*, 255501.

[81] A. H. Kitai, *Solid State Luminescence: Theory, Materials and Devices*, Springer Science & Business Media, **2012**.

[82] S. Lee, T. Kang, W. Lee, M. M. Afandi, J. Ryu, J. Kim, *Sci. Rep.* **2018**, *8*, 301.

[83] S. Lee, T. Kang, W. Lee, M. M. Afandi, J. Ryu, J. Kim, S. Son, *Phys. Status Solidi Appl. Mater. Sci.* **2018**, *215*, 1701071.

[84] G. Horowitz, *Adv. Mater.* **1998**, *10*, 365.

[85] H. Sirringhaus, *Adv. Mater.* **2014**, *26*, 1319.

[86] T. Someya, T. Sekitani, S. Iba, Y. Kato, H. Kawaguchi, T. Sakurai, *Proc. Natl. Acad. Sci.* **2004**, *101*, 9966.

[87] J. T. Mabeck, G. G. Malliaras, *Anal. Bioanal. Chem.* **2006**, *384*, 343.

[88] R. Rotzoll, S. Mohapatra, V. Olariu, R. Wenz, M. Grigas, K. Dimmler, O. Shchekin, A. Dodabalapur, *Appl. Phys. Lett.* **2006**, *88*, 123502.

[89] M. Muccini, *Nat. Mater.* **2006**, *5*, 605.

[90] C. Di, F. Zhang, D. Zhu, *Adv. Mater.* **2013**, *25*, 313.

[91] I. Graz, M. Krause, S. Bauer-Gogonea, S. Bauer, S. P. Lacour, B. Ploss, M. Zirkl, B. Stadlober, S. Wagner, *J. Appl. Phys.* **2009**, *106*, 34503.

[92] S. Hannah, A. Davidson, I. Glesk, D. Uttamchandani, R. Dahiya, H. Gleskova, *Org. Electron.* **2018**, *56*, 170.

[93] F. A. Viola, A. Spanu, P. C. Ricci, A. Bonfiglio, P. Cosseddu, *Sci. Rep.* **2018**, *8*, 8073.

[94] N. Lu, D.-H. Kim, *Soft Robot.* **2014**, *1*, 53.

[95] V. P. Plessky, L. M. Reindl, *IEEE Trans. Ultrason. Ferroelectr. Freq. Control* **2010**, *57*, 654.

[96] G. Wingqvist, *Surf. Coatings Technol.* **2010**, *205*, 1279.

[97] K. M. Lakin, *IEEE Microw. Mag.* **2003**, *4*, 61.

[98] E. Benes, M. Gröschl, W. Burger, M. Schmid, *Sensors Actuators A Phys.* **1995**, *48*, 1.

[99] B. Drafts, *IEEE Trans. Microw. Theory Tech.* **2001**, *49*, 795.

[100] T. Manzaneque, V. Ruiz-Díez, J. Hernando-García, E. Wistrela, M. Kucera, U. Schmid, J. L. Sánchez-Rojas, *Sensors Actuators A Phys.* **2014**, *220*, 305.

[101] H.-C. Chang, S.-S. Hung, Y.-H. Chen, M.-H. Tsai, in *5th Int. Conf. Inf. Eng. Mech. Mater.*, **2015**, pp. 440–444.

[102] Y. Chen, P. I. Reyes, Z. Duan, G. Saraf, R. Wittstruck, Y. Lu, O. Taratula, E. Galoppini, in *J. Electron. Mater.*, **2009**.

[103] Y.-C. Chen, W.-T. Chang, K.-S. Kao, C.-H. Yang, C.-C. Cheng, *J. Nanomater.* **2013**,

2013, 2.

[104] H. Zhao, X. Guo, Y. Wang, X. Duan, H. Qu, H. Zhang, D. Zhang, W. Pang, *Sensors Actuators B Chem.* **2016**, *223*, 83.

[105] Y. Chang, N. Tang, H. Qu, J. Liu, D. Zhang, H. Zhang, W. Pang, X. Duan, *Sci. Rep.* **2016**, *6*, 23970.

[106] R. Abdolvand, B. Bahreyni, J. E.-Y. Lee, F. Nabki, *Micromachines* **2016**, *7*, 160.

[107] J. Yan, X. Guo, S. Duan, P. Jia, L. Wang, C. Peng, S. Zhang, *Sensors* **2015**, *15*, 27804.

[108] K. Gurnett, T. Adams, *III-Vs Rev.* **2006**, *19*, 38.

[109] J. Zhou, S. Dong, H. Jin, B. Feng, D. Wang, *J. Control Sci. Eng.* **2012**, *2012*, 5.

[110] Y. Jiang, M. Zhang, X. Duan, H. Zhang, W. Pang, *Appl. Phys. Lett.* **2017**, *111*, 023505.

[111] D. Rus, M. T. Tolley, *Nature* **2015**, *521*, 467.

[112] V. A. Ho, M. Makikawa, S. Hirai, *IEEE Sens. J.* **2013**, *13*, 4065.

[113] S. Coyle, K. T. Lau, N. Moyna, D. O'Gorman, D. Diamond, F. Di Francesco, D. Costanzo, P. Salvo, M. G. Trivella, D. E. De Rossi, N. Taccini, R. Paradiso, J. A. Porchet, A. Ridolfi, J. Luprano, C. Chuzel, T. Lanier, F. Revol-Cavalier, S. Schoumacker, V. Mourier, I. Chartier, R. Convert, H. De-Moncuit, C. Bini, *IEEE Trans. Inf. Technol. Biomed.* **2010**, *14*, 364.

[114] L. M. Castano, A. B. Flatau, *Smart Mater. Struct.* **2014**, *47*, 053001.

[115] C. Gonçalves, A. Ferreira da Silva, J. Gomes, R. Simoes, *Inventions* **2018**, *3*, 14.

[116] J. Lee, H. Kwon, J. Seo, S. Shin, J. H. Koo, C. Pang, S. Son, J. H. Kim, Y. H. Jang, D. E. Kim, T. Lee, *Adv. Mater.* **2015**, *27*, 2433.

[117] A. L. Leon, L. R. Manea, L. Hristian, *IOP Conf. Ser. Mater. Sci. Eng.* **2016**, *145*, DOI 10.1088/1757-899X/145/3/032005.

[118] M. Baima, T. Andrew, *Fibers* **2018**, *6*, 41.

[119] K. Cherenack, C. Zysset, T. Kinkeldei, N. Münzenrieder, G. Tröster, *Adv. Mater.* **2010**, *22*, 5178.

[120] X. Li, P. Sun, L. Fan, M. Zhu, K. Wang, M. Zhong, J. Wei, D. Wu, Y. Cheng, H. Zhu, *Sci. Rep.* **2012**, *2*, 395.

[121] L. Motha, J. Kim, W. S. Kim, *Org. Electron. physics, Mater. Appl.* **2015**, *23*, 82.

[122] K. Lei, K. Lee, M. Lee, *Microelectron. Eng.* **2012**, *99*, 1.

[123] G. Firpo, E. Angeli, L. Repetto, U. Valbusa, *J. Memb. Sci.* **2015**, *481*, 1.

[124] M. Amjadi, K. U. Kyung, I. Park, M. Sitti, *Adv. Funct. Mater.* **2016**, DOI 10.1002/adfm.201504755.

[125] J. A. Rogers, T. Someya, Y. Huang, *Science (80-.).* **2010**, DOI 10.1126/science.1182383.

[126] R. Cao, X. Pu, X. Du, W. Yang, J. Wang, H. Guo, S. Zhao, Z. Yuan, C. Zhang, C. Li, Z. L. Wang, *ACS Nano* **2018**, *12*, 5190.

[127] W. Yuan, J. Yang, K. Yang, H. Peng, F. Yin, *ACS Appl. Mater. Interfaces* **2018**, *10*, 19906.

[128] U. Koc, G. Y. Karaca, A. U. Oksuz, L. Oksuz, *J. Mater. Sci. Mater. Electron.* **2017**, *28*, 8725.

[129] F. Gong, C. Meng, J. He, X. Dong, *Prog. Org. Coatings* **2018**, *121*, 89.

[130] A. Kaynak, S. S. Najar, R. C. Foitzik, *Synth. Met.* **2008**, *158*, 1.

[131] Z. H. Lim, Z. X. Chia, M. Kevin, A. S. W. Wong, G. W. Ho, *Sensors Actuators, B Chem.* **2010**, *151*, 121.

[132] A. Ali, V. Baheti, J. Militky, Z. Khan, S. Q. Z. Gilani, *Fibers Polym.* **2018**, *19*, 607.

[133] J. Ryu, J. Kim, J. Oh, S. Lim, J. Y. Sim, J. S. Jeon, K. No, S. Park, S. Hong, *Nano Energy* **2018**, DOI https://doi.org/10.1016/j.nanoen.2018.10.071.

[134] Y. Zhu, S. Murali, W. Cai, X. Li, J. W. Suk, J. R. Potts, R. S. Ruoff, *Adv. Mater.* **2010**, *22*, 3906.

[135] F. Meng, W. Lu, Q. Li, J. H. Byun, Y. Oh, T. W. Chou, *Adv. Mater.* **2015**, *27*, 5113.

[136] H. Cheng, C. Hu, Y. Zhao, L. Qu, *NPG Asia Mater.* **2014**, *6*, e113.

[137] J. Molina, *RSC Adv.* **2016**, *6*, 68261.

[138] D. Wang, D. Li, M. Zhao, Y. Xu, Q. Wei, *Appl. Surf. Sci.* **2018**, *454*, 218.

[139] X. Hu, M. Tian, L. Qu, S. Zhu, G. Han, *Carbon N. Y.* **2015**, *95*, 625.

[140] H. Souri, D. Bhattacharyya, *ACS Appl. Mater. Interfaces* **2018**, *10*, 20845.

[141] Z. L. Wang, T. Jiang, L. Xu, *Nano Energy* **2017**, *39*, 9.

[142] S. J. Kim, W. Song, Y. Yi, B. K. Min, S. Mondal, K. S. An, C. G. Choi, *ACS Appl. Mater. Interfaces* **2018**, *10*, 3921.

[143] J. C. Yeo, Z. Liu, Z. Q. Zhang, P. Zhang, Z. Wang, C. T. Lim, *Adv. Mater. Technol.* **2017**, *2*, 1700006.

[144] M. D. Dickey, *Adv. Mater.* **2017**, *29*, 1606425.

[145] F. Geiger, C. A. Busse, R. I. Loehrke, *Int. J. Thermophys.* **1987**, *8*, 425.

[146] C. B. Cooper, K. Arutselvan, Y. Liu, D. Armstrong, Y. Lin, M. R. Khan, J. Genzer, M. D. Dickey, *Adv. Funct. Mater.* **2017**, *27*, 1605630.

[147] D. Zrnic, D and Swatik, *J. less common Met.* **1969**, *18*, 67.

[148] S. Zhu, J. H. So, R. Mays, S. Desai, W. R. Barnes, B. Pourdeyhimi, M. D. Dickey, *Adv. Funct. Mater.* **2013**, *23*, 2308.

[149] I. D. Joshipura, H. R. Ayers, C. Majidi, M. D. Dickey, *J. Mater. Chem. C* **2015**, *3*, 3834.

[150] K. Spells, *Proc. Phys. Soc.* **1936**, *48*, 299.

[151] J. B. Chossat, Y. L. Park, R. J. Wood, V. Duchaine, *IEEE Sens. J.* **2013**, *13*, 3405.

[152] Y. L. Park, B. R. Chen, R. J. Wood, *IEEE Sens. J.* **2012**, *12*, 2711.

[153] C. Laschi, B. Mazzolai, M. Cianchetti, *Sci. Robot.* **2016**, *1*, eaah3690.

[154] Y. Mengüç, Y. L. Park, H. Pei, D. Vogt, P. M. Aubin, E. Winchell, L. Fluke, L. Stirling, R. J. Wood, C. J. Walsh, *Int. J. Rob. Res.* **2014**, *33*, 1748.

[155] T. Yang, D. Xie, Z. Li, H. Zhu, *Mater. Sci. Eng. R Reports* **2017**, *115*, 1.

[156] H. B. Cott, *Adaptive Coloration in Animals*, Methuen; London, **1940**.

[157] J. W. Bradbury, S. L. Vehrencamp, **1998**.

[158] Y. Fu, C. A. Tippets, E. U. Donev, R. Lopez, *Wiley Interdiscip. Rev. Nanomedicine Nanobiotechnology* **2016**, *8*, 758.

[159] J. Teyssier, S. V Saenko, D. Van Der Marel, M. C. Milinkovitch, *Nat. Commun.* **2015**, *6*, 6368.

[160] R. Hanlon, *Curr. Biol.* **2007**, *17*, R400.

[161] M. D. Fairchild, **2005**.

[162] H. K. Bisoyi, T. J. Bunning, Q. Li, *Adv. Mater.* **2018**, 1706512.

[163] E. Armstrong, C. O'Dwyer, *J. Mater. Chem. C* **2015**, *3*, 6109.

[164] S. John, *Phys. Rev. Lett.* **1987**, *58*, 2486.

[165] E. Yablonovitch, *Phys. Rev. Lett.* **1987**, *58*, 2059.

[166] J. D. Joannopoulos, S. G. Johnson, J. N. Winn, R. D. Meade, *Photonic Crystals: Molding the Flow of Light*, Princeton University Press, **2011**.

[167] L. Lu, J. D. Joannopoulos, M. Soljačić, *Nat. Photonics* **2014**, *8*, 821.

[168] Y. Liu, A. A. Houck, *Nat. Phys.* **2017**, *13*, 48.

[169] I. Aharonovich, D. Englund, M. Toth, *Nat. Photonics* **2016**, *10*, 631.

[170] P. Lodahl, S. Mahmoodian, S. Stobbe, *Rev. Mod. Phys.* **2015**, *87*, 347.

[171] J. V Sanders, *Nature* **1964**, *204*, 1151.

[172] J. M. Weissman, H. B. Sunkara, S. T. Albert, S. A. Asher, *Science (80-.).* **1996**, *274*, 959.

[173] J. Ge, Y. Yin, *Angew. Chemie Int. Ed.* **2011**, *50*, 1492.

[174] Y. Kang, J. J. Walish, T. Gorishnyy, E. L. Thomas, *Nat. Mater.* **2007**, *6*, 957.

[175] N. Vogel, M. Retsch, C.-A. Fustin, A. del Campo, U. Jonas, *Chem. Rev.* **2015**, *115*, 6265.

[176] Y. Yue, T. Kurokawa, M. A. Haque, T. Nakajima, T. Nonoyama, X. Li, I. Kajiwara, J. P. Gong, *Nat. Commun.* **2014**, *5*, 4659.

[177] N. Akamatsu, W. Tashiro, K. Saito, J. Mamiya, M. Kinoshita, T. Ikeda, J. Takeya, S. Fujikawa, A. Priimagi, A. Shishido, *Sci. Rep.* **2014**, *4*, 5377.

[178] H. Guo, J. Tang, K. Qian, D. Tsoukalas, M. Zhao, J. Yang, B. Zhang, X. Chou, J. Liu, C. Xue, *Sci. Rep.* **2016**, *6*, 23606.

[179] N. Akamatsu, M. Fukuhara, S. Fujikawa, A. Shishido, *J. Photopolym. Sci. Technol.* **2018**, *31*, 523.

[180] M. Mitov, *Adv. Mater.* **2012**, *24*, 6260.

[181] D. J. Broer, J. Lub, G. N. Mol, *Nature* **1995**, *378*, 467.

[182] J. Xiang, Y. Li, Q. Li, D. A. Paterson, J. M. D. Storey, C. T. Imrie, O. D. Lavrentovich, *Adv. Mater.* **2015**, *27*, 3014.

[183] A. Ryabchun, A. Bobrovsky, *Adv. Opt. Mater.* **2018**, 1800335.

[184] Y. Li, Y. Liu, D. Luo, *Opt. Express* **2017**, *25*, 26349.

[185] J.-D. Lin, H.-L. Lin, H.-Y. Lin, G.-J. Wei, Y.-C. Chuang, L.-J. Chen, S.-Y. Huang, C.-Y. Huang, T.-S. Mo, C.-R. Lee, *J. Mater. Chem. C* **2017**, *5*, 3222.

[186] J. Tian, Y. He, J. Li, J. Wei, G. Li, J. Guo, *Adv. Opt. Mater.* **2018**, *6*, 1701337.

[187] T. J. White, D. J. Broer, *Nat. Mater.* **2015**, *14*, 1087.

[188] B. Taheri, A. F. Munoz, P. Palffy-Muhoray, R. Twieg, *Mol. Cryst. Liq. Cryst. Sci. Technol. Sect. A. Mol. Cryst. Liq. Cryst.* **2001**, *358*, 73.

[189] H. Finkelmann, S. T. Kim, A. Munoz, P. Palffy-Muhoray, B. Taheri, *Adv. Mater.* **2001**, *13*, 1069.

[190] P. V Shibaev, C. Schlesier, R. Uhrlass, S. Woodward, E. Hanelt, *Liq. Cryst.* **2010**, *37*, 1601.

[191] O. T. Picot, M. Dai, E. Billoti, D. J. Broer, T. Peijs, C. W. M. Bastiaansen, *RSC Adv.* **2013**, *3*, 18794.

[192] E. P. A. van Heeswijk, J. J. H. Kloos, J. de Heer, T. Hoeks, N. Grossiord, A. P. H. J. Schenning, *ACS Appl. Mater. Interfaces* **2018**, *10*, 30008.

[193] A. J. J. Kragt, D. J. Broer, A. P. H. J. Schenning, *Adv. Funct. Mater.* **2018**, *28*, 1704756.

[194] D. A. Davis, A. Hamilton, J. Yang, L. D. Cremar, D. Van Gough, S. L. Potisek, M. T. Ong, P. V Braun, T. J. Martínez, S. R. White, *Nature* **2009**, *459*, 68.

[195] Y. Chen, A. J. H. Spiering, S. Karthikeyan, G. W. M. Peters, E. W. Meijer, R. P. Sijbesma, *Nat. Chem.* **2012**, *4*, 559.

[196] J. Li, C. Nagamani, J. S. Moore, *Acc. Chem. Res.* **2015**, *48*, 2181.

[197] S. L. Potisek, D. A. Davis, N. R. Sottos, S. R. White, J. S. Moore, *J. Am. Chem. Soc.* **2007**, *129*, 13808.

[198] M. M. Caruso, D. A. Davis, Q. Shen, S. A. Odom, N. R. Sottos, S. R. White, J. S. Moore, *Chem. Rev.* **2009**, *109*, 5755.

[199] A. Lavrenova, D. W. R. Balkenende, Y. Sagara, S. Schrettl, Y. C. Simon, C. Weder, *J. Am. Chem. Soc.* **2017**, *139*, 4302.

[200] G. A. Filonenko, J. R. Khusnutdinova, *Adv. Mater.* **2017**, *29*, 1700563.

[201] N. A. Atari, *Phys. Lett. A* **1982**, *90*, 93.

[202] Y. Fujio, C.-N. Xu, Y. Terasawa, Y. Sakata, J. Yamabe, N. Ueno, N. Terasaki, A. Yoshida, S. Watanabe, Y. Murakami, *Int. J. Hydrogen Energy* **2016**, *41*, 1333.

[203] D. Tu, C. Xu, A. Yoshida, M. Fujihala, J. Hirotsu, X. Zheng, *Adv. Mater.* **2017**, *29*, 1606914.

[204] J. T. Muth, D. M. Vogt, R. L. Truby, Y. Mengüç, D. B. Kolesky, R. J. Wood, J. A. Lewis, *Adv. Mater.* **2014**, *26*, 6307.

[205] Y. Xu, X. Wu, X. Guo, B. Kong, M. Zhang, X. Qian, S. Mi, W. Sun, *Sensors* **2017**, *17*, 1166.

[206] S. Tibbits, *Archit. Des.* **2014**, *84*, 116.

Table 1. Materials and properties in multi-functional sensors

Materials	Mechanism	Substrate	Sensitivity/Resolution			Applications	Ref
			Force	Temperature	Others		
Piezoelectric or pyroelectric							
PZT/PDMS	Piezoelectric	PDMS	694 mV/N(Pressure) 455 mV/N(Shear)	-	-	Pressure, strain, shear sensors	[54]
PVDF	Piezoelectric	PDMS	6.5 $VkPa^{-1}$ (1-8.3kPa)	-	-	Medical diagnosis, walking sensor	[57]
PVDF	Pyroelectric	Free standing	-	-	-	Breathing sensor, temperature sensor	[61]
Piezoelectric & pyroelectric							
ZnO/PVDF	Piezo- and pyro-electric	Free standing	0.062 Ω/10 Pa	Smallest pressure 10Pa	-	Artificial e-skin	[65]
BaTiO3/PVDF-TrFE	Piezo- and pyro-electric	Polyimide	0.22 nF/N	~54pF/°C	-	Artificial e-skin	[68]
0.7PMN-0.3PT	Piezo- and pyro-electric	PET	-	-	-	Acoustic sound, human motion, water flow, light illumination	[69]
Piezoelectric & piezoresistive							
ZnO	Piezoresistive	PDMS	$-0.768\ kPa^{-1}$	−0.70%/◦C	-	Artificial e-skin	[66]
AZO	Piezoresistive	PDMS	$-0.223\ kPa^{-1}$	-0.69%/◦C	-	Artificial e-skin	
ZnO/PDMS AgNWs/PEDOT:PSS/PDMS	Piezo- and Pyro-electric, Piezoresistive	PDMS	(Stretching motion) ~3400%/4 mm	~0.52%/°C	-	Movement and temperature sensor	[64]
cotton@SWCNTs /ZnO@PVDF	Piezoelectric, piezoresisitve	Cotton	(Fluid pressure) 0.002 V/Pa	~−0.025 ΔR/ R0/°C	-	Electronic blood vessels	[67]
PVDF-rGO	Piezo- and Pyro-electric, Piezoresistive	PET	35 μA/Pa (<2.45 kPa) and 5 μA/Pa (2.45 to 17.15 kPa)	3.3%/°C	-	Robotic skins, wearable sensors, and medical diagnostic devices	[73]
PVDF-rGO	Piezoelectric	PET	47.7 kPa-1 1.3 Pa minimum detection	-	-	Artificial e-skin	[55]
PAN-C/BTO	Piezoelectric, piezoeresistive, triboelectric	PDMS	$1.44\ V{\cdot}N^{-1}$ (0.15-20N)	1.12 /°C (58.9° to 120.2°)	-	Human swallowing, waking gaits, finger flexure and tapping	[58]
Piezoelectric & other mechanisms							
PVDF	Piezoelectric, electrostatic	Free standing	-	-	-	Tactile sensor, identify materials	[75]
PVDF/CI	Piezoelectric, magnetic	PDMS	-	-	$Y = -3.99*10-4X^2 + 1.52X-59.95$ (X:magnetic flux density, Y:charges)	Deformation sensor, magnetic field sensor	[77]
ZnO	Piezoelectric, photoelectric	Glass	-	-	-	UV photodetection, H_2 gas sensing	[78]
ZnO-NiO	Piezoelectric, Piezo-phototronic effect	Ni foil	-	-	-	Photodetector	[79]

Ppy/PVDF	Piezoelectric	Free standing		-	-	Photo-detector, vision substitution	[80]
ZnS/PZT	Piezoelectric, Electroluminescent	Copper Brass	Sound pressre value 88 dB at 100V	73 dB (25°C), 65 dB (250°C)	-	Remote stress sensor	[82]
ZnS/PVDF	Piezoelectric, Electroluminescent	PVDF	Sound pressre value 56 dB at 100V	52 dB (25°C), 42 dB (100°C).	-	Emergency warning system, advertising panel, and remote stress sensor	[83]
Transistors or resonator							
PbTiO nanoparticles in PVDF-TrFE	Capacitance	Polyimide	-	-	Low cross-sensitivity	E-skin	[91]
PVDF-TrFE	Capacitance	Si	~7.5 pF/N	~7 pF/°C	-	E-skin, electronic-textiles	[92]
PVDF	Ferroelectric	Parylene C	6 nA/N	70 nA/°C	-	E-skin, epidermal electronics	[93]
PVDF-TrFE/$BaTiO_3$	Piezo- and pyro-electric, thermoresistive	Polyimide	2.615 mV kPa^{-1}	-	-	E-skin	[6]
PVDF-TrFE	Piezo- and pyro-electric, thermoresistive	Polyimide	1.02kPa^{-1} (static) 0.028kPa^{-1} (dynamic)	-	-	E-skin	[7]
$LiNbO_3$	Piezo- and pyro-electric, SAW frequency and propagation speed shift	$LiNbO_3$	8.19 kHz/bar	4.05 kHz/ºC	-	Tire Pressure and temperature sensor	[101]
AlN	Piezoelectric, Multimode resonance	Si	-	-	2295 $Hzcm^2$/ng for longitudinal and 1363 $Hzcm^2$/ng for shear mode	Liquid sensing applications	[103]
AlN	Piezoelectric, Out-of-plane resonance mode	Si	-	-	1.83×10^{-7} g/ml for density and 1.74×10^{-5} mPas for viscosity - measurement	Density-viscosity sensor in liquid	[100]
ZnO functionalized with DNA	Piezoelectric, Resonant frequency shift by Mass loading	Si	-	-	Mass sensitivity of 1.72×10^3 $Hzcm^2$/ng	Biosensor	[102]
AlN functionalized with trimethoxy (octadecyl) silane	Piezoelectric, Multiple resonant modes, Mass-sensitive frequency shift	Si	-	-	Sensitivities of different modes on the same region are different	E-nose for gas sensing	[26]
AlN functionalized with self-assembled monolayers	Piezoelectric, Mass-sensitive frequency shift	Si	-	-	Trace level	E-nose for gas sensing	[105]
AlN functionalized with SWCNT-PDDA/GOD	Piezoelectric, Mass-sensitive frequency shift	Si	-	-	Mass:0.84 $MHzcm^2$/g Glucose concentration: 0.78 nA/(mMmm2). Viscosity: 0.422 mΩ/mM	Glucose monitoring	[104]
Conductive fabric							
Steel	Piezoresistive	PDMS	-	-	-	Under-foot monitoring	-
Graphene	Piezoresistive	PDMS	GF=10^3 (2-6% strain) GF=10^6 (>7% strain)				[120]
Silver/copper	Piezoresistive	Cotton					[132]

Silver nanoparticles/poly(styrene -block-butadienstyrene) coated poly(p-phenylene terephthalamide) fiber	Capacitance	PDMS	0.21 kPa^{-1}(<2kPa) 0.064 kPa^{-1} (>2kPa)	-	-	Wearable human-machine interface, smart gloves, clothes	[116]
PEDOT:PSS/DMSO	Electrothermal	PET fabrics	-	-	-	Portable heater	[129]
PVDF-TrFE/PDMS with MWCNT/PEDOT:PSS	Piezoelectric	PDMS	GF=80-177 (0-50% strain)	-	-	Precise monitoring of motion, detect tactile inputs, power source	[133]
Graphene	Piezoresistive	PU/polyamide	72 kPa^{-1}	-	-	Physiological signal monitoring	[127]
GNP/CB	Piezoresistive, electrothermal	Cotton/Wool fabrics	GF= 20.4	-	-	Human-machine interaction electronics, wearable heater	[140]
CNT/PU	Triboelectric	Nylon	0.048 kPa^{-1}	-	-	Gesture sensors, wireless control devices	[126]
SWCNT/rGO	Piezoresistive	PET	GF = 5.4	-	-	Smart gloves	[142]
Liquid metal							
EGaIn	Piezoresistive	PDMS	~4 kPa^{-1}	-	-	Flexible display, electronic textile, soft robotics, consumer healthcare	[29]
EGaIn	Piezoresistive	Silicone rubber	GF=3.6 for x-axis GF=3.7 for y-axis	-	-	E-skin	[152]
EGaIn	Piezoresistive	Silicone rubber	37mV/N, -28.6mV/N for in-plane force 27.8mV/N, 572mV/N for normal force	-	-	Testing robotic hand grasping, detect slippage and grasp failure	[30]
eGaIn	Piezoresistive	PDMS	-	-	-	E-skin, observe pose in soft robotic system	[31]
Photonic crystals							
PDGI/PAAm hydrogel	Reflection from the gel in response to mechanical compression	Free standing	~0.1 nm Pa^{-1}(Pressure range <3 kPa)	-	Mechanical stability: $>10^4$ cycling test Ultrafast-response time: <0.1 ms Reversible color spectra: 340-640 nm High spatial resolution: ~10 mm)	Flexible display, stress sensor, sensor for the contractile force of cells, telecommunication device	[176]
Cholesteric liquid crystals							
Dye-doped cholesteric liquid crystal elastomer	Lasing from the elastomer in response to mechanical strain	Free standing	-	-	-	Strain sensor, laser	[189]
Crosslinked cholesteric liquid crystal film	Reflection from film gel in response to mechanical extension	Polyamide -6	3nm/% strain	-	Time dependent optical response	Strain sensor	[191]

Mechanochromic							
$Li_xNbO_3:Pr_3^+$	Piezoluminescence (elasticoluminescence)	–	High sensitivity in the range of <100 μst strain	-	No threshold for stress sensing. Continuous autoluminescence under more than 100 cycles	Microstress sensing, damage diagnosis, electro-mechano-optical energy conversion	[203]

Mengying Xie has a BSc degree in Applied Physics from Tianjin University, China (2006–2010) and a PhD in Mechatronics Engineering from the University of Auckland, New Zealand (2010–2015). Later she worked in NEMESIS project in University of Bath as a postdoc (2016-2018). In 2018 she joined Ritsumeikan University as a senior researcher. Her research area includes energy harvesting and its applications, including water splitting, self-powered sensors and other wearable electronics.

Kyohei Hisano has a BSc degree in Chemistry from Tokyo University of Science, Japan (2009–2013) and a PhD from the Tokyo Institute of Technology (Tokyo Tech) under the guidance of Prof. Shishido in 2018. In 2018, he joined Ritsumeikan University as an assistant professor. His PhD work exploited the novel technology to inscribe arbitrary molecular orientation patterns in functional polymeric materials, and designed photonic and mechanic applications applicable to soft robotics, flexible displays, and super-resolution imagings. His research interests include hierarchical molecular orientation design and control for functional materials and devices in the field of optics, photonics, and mechanics.

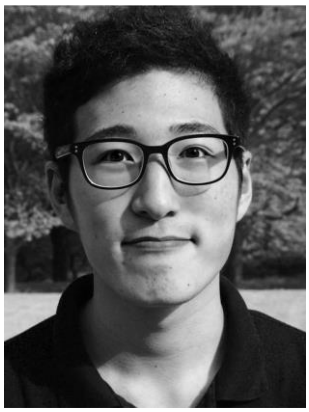

Christopher Rhys Bowen has a BSc degree in Materials Science from the University of Bath (1986–1990) and a DPhil from the University of Oxford (1990–1993). Post-doctoral work was at Tecnische Universität Harburg-Hamburg and University of Leeds (1994–1996). He was Senior Scientist at the Defence Evaluation and Research Agency from 1996–1998. He joined Bath as a Lecturer in 1998 and is now Professor of Materials and ERC Advanced Investigator, ERC Grant Agreement No. 320963 on Novel Energy Materials, Engineering Science and Integrated Systems (NEMESIS). Research includes energy harvesting, ferroelectrics and functional ceramics.

Flexible multi-functional sensors can provide intelligent sensing for wearable and human-machine interacting robots. This review focuses on recent progress in the development and advancement of flexible and multi-functional sensors based on a range of sensory mechanisms and materials including piezoelectric, conductive and optical materials. Potential future research directions and challenges are discussed.

multi-functional sensors, flexible, piezoelectric, piezoresistive, optical

Mengying Xie*, Kyohei Hisano, Mingzhu Zhu, Takuya Toyoshi, Min Pan, Shima Okada, Osamu Tsutsumi, Sadao Kawamura, Chris Bowen

Flexible multi-functional sensors for wearable and robotic applications